

MULTILINEAR POD-DEIM MODEL REDUCTION FOR 2D AND 3D SEMILINEAR SYSTEMS OF DIFFERENTIAL EQUATIONS

GERHARD KIRSTEN*

Dipartimento di Matematica, Universit'a di Bologna
Piazza di Porta S. Donato, 5
I-40127 Bologna, Italy

ABSTRACT. We are interested in the numerical solution of coupled semilinear partial differential equations (PDEs) in two and three dimensions. Under certain assumptions on the domain, we take advantage of the Kronecker structure arising in standard space discretizations of the differential operators and illustrate how the resulting system of ordinary differential equations (ODEs) can be treated directly in matrix or tensor form. Moreover, in the framework of the proper orthogonal decomposition (POD) and the discrete empirical interpolation method (DEIM) we derive a two- and three-sided model order reduction strategy that is applied directly to the ODE system in matrix and tensor form respectively. We discuss how to integrate the reduced order model and, in particular, how to solve the tensor-valued linear system arising at each timestep of a semi-implicit time discretization scheme. We illustrate the efficiency of the proposed method through a comparison to existing techniques on classical benchmark problems such as the two- and three-dimensional Burgers equation.

1. Introduction. We are interested in the computationally efficient numerical solution of systems of semilinear partial differential equations (PDEs) of the form

$$\begin{cases} \dot{u}_1 = \mathcal{L}_1(u_1) + f_1(\nabla u_1, u_1, \dots, u_g, t) \\ \vdots \\ \dot{u}_g = \mathcal{L}_g(u_g) + f_g(\nabla u_g, u_1, \dots, u_g, t), \end{cases} \quad (1)$$

where $u_i = u_i(\mathbf{x}, t)$, with $\mathbf{x} \in \Omega \subset \mathbb{R}^d$, $t \in [0, t_f]$ and suitable initial and boundary conditions, for all $i = 1, 2, \dots, g$. We restrict our attention to the two-dimensional and three-dimensional cases, that is $d = 2, 3$. In this setting we assume that $\mathcal{L}_i : \Omega \rightarrow \mathbb{R}$ is linear in u_i , typically a diffusion operator, whereas $f_i : \Omega \times [0, t_f] \rightarrow \mathbb{R}$ is assumed to be nonlinear in $(\nabla u_i, u_1, \dots, u_g)$ and t . PDEs of the form **1** describe mathematical models in several scientific fields, such as chemistry [13, 51], biology [37, 23, 18] and medicine [45]. For further applications we point the reader to [33],[34],[42],[50], and references therein.

The simulation of **1** and the accurate approximation to its solution pose several computational challenges. A semi-discretization in space of **1** leads to a discrete approximation of the PDE inside a hypercube in \mathbb{R}^d . The discrete model can then

2020 *Mathematics Subject Classification.* Primary: 37M99, 15A21, 15A24, 15A69 65N06.

Key words and phrases. Proper orthogonal decomposition, Discrete empirical interpolation method, semilinear tensor differential equations, semi-implicit time integration, coupled systems of differential equations.

The author is a member of Indam-GNCS, which support is gratefully acknowledged.

be integrated in time, most commonly by a time-discretization scheme, such as Implicit-Explicit schemes for instance [2, 43]. The method of lines (MOL) based on space discretizations, such as finite differences, finite elements, spectral methods, isogeometric analysis, rewrites the system 1 as a system of ODEs of the form

$$\begin{cases} \dot{\mathbf{u}}_1(t) &= \mathbf{L}_1 \mathbf{u}_1(t) + \mathbf{f}_1(\mathbf{D}_1 \mathbf{u}_1, \mathbf{u}_1, \dots, \mathbf{u}_g, t), \\ &\vdots \\ \dot{\mathbf{u}}_g(t) &= \mathbf{L}_g \mathbf{u}_g(t) + \mathbf{f}_g(\mathbf{D}_g \mathbf{u}_g, \mathbf{u}_1, \dots, \mathbf{u}_g, t), \end{cases} \quad (2)$$

where $\mathbf{u}_i \in \mathbb{R}^N$ and each function $\mathbf{f}_i : \mathbb{R}^N \times \mathbb{R}^N \times \dots \times \mathbb{R}^N \times [0, t_f] \rightarrow \mathbb{R}^N$ represents the function f_i evaluated at the entries of the set of vectors $\{\mathbf{u}_i\}_{i=1}^g$ and $\mathbf{D}_i \mathbf{u}_i$. In this setting, $\mathbf{L}_i \in \mathbb{R}^{N \times N}$ accounts for the discretization of the linear operator \mathcal{L}_i on the selected basis and $\mathbf{D}_i \in \mathbb{R}^{N \times N}$ for that of the gradient. Furthermore, if finite differences are considered, then $N = \prod_{i=1}^d n_i$, where n_i represents the number of spatial nodes in the x_i direction. It is clear that even for moderate n_i the dimension of the considered matrices and vectors are very large when $d = 2, 3$. Furthermore, in many cases fine grid discretizations of the system are required for an accurate simulation (see e.g., [9]). This poses a massive computational and memory challenge for systems of the form 2.

As a result, model order reduction techniques have been applied to dramatically reduce the dimension and the complexity of the resulting system of ODEs, see e.g., [9, 53, 26, 44, 25, 27, 30]. In particular, the common approach is to form a lexicographic ordering of the spatial nodes, unrolling the arrays (i.e., matrices or tensors when $d = 2$ and $d = 3$ respectively) of nodal values into long vectors in \mathbb{R}^N , i.e., the unknown vectors $\mathbf{u}_i(t) \in \mathbb{R}^N$. The dimension of the state space is then reduced to say $k \ll N$ through projection onto a low-dimensional subspace. Techniques for dimension reduction include the proper orthogonal decomposition (POD) [6],[5],[22],[32], reduced basis methods, see, e.g., [41], and rational interpolation strategies [1] to mention a few. Furthermore, the complexity of the reduced model can be further decreased through hyper-reduction of the nonlinear term. This includes methods such as Missing Point Estimation (MPE) [3], the best points interpolation method (BPIM) [39], and the discrete empirical interpolation method (DEIM) [8], which is based on the Empirical Interpolation Method (EIM), originally introduced in [4]. Another model reduction approach is presented in [31]. Here, the authors avoid the hyper-reduction step by rewriting the nonlinear term in polynomial form, through so-called lifting transformations; see e.g., [20]. The dimension of the resulting model is then fully reduced by POD.

The success of the reduced order modelling is due to the fact that the solution trajectories are commonly attracted to low-dimensional manifolds [8]. These low-dimensional models can then be rapidly simulated in a so-called online phase to form an approximation to the solution at the required timesteps. A shortcoming of the existing procedures, however, is the massive computational and storage demand in the offline phase. Even in the online phase, several vectors of length N need to be stored in order to lift the low-dimensional functions back to the full dimension. In this paper we aim to address precisely this shortcoming, with particular focus on POD for dimension reduction and DEIM for interpolation of the nonlinear function.

To this end, we illustrate that under certain hypotheses on the operators and the discretization basis in particular domains, 2 can be equivalently expressed and integrated in array form, without forming a lexicographical ordering of the spatial

nodes. In addition to a better structural interpretation of the discrete quantities, this can also lead to reduced memory requirements and computational costs. We discuss how to integrate the system in array form, and particularly also how to solve the tensor-structured linear system arising from the semi-implicit time integration when $d = 3$.

Furthermore, inspired by [28], we apply a d -sided POD-DEIM model order reduction, directly to the discrete system in array form, which is particularly advantageous, since no mapping is required from $\mathbb{R}^{n_1 \times \dots \times n_d}$ to \mathbb{R}^N , and hence only vectors of length n_1, \dots, n_d need to be stored and processed. We mention that in the Arxiv report [28, Section 8] the authors also present one example where a two-sided POD-DEIM order reduction strategy is applied to systems of matrix-valued ODEs. The presentation in this paper is, however, more general as it extends this idea to the higher dimensional multilinear array setting, including first order nonlinearities. Furthermore, a more in-depth experimental analysis of the two-dimensional case is presented than in [28].

The paper is organized as follows. In section 2 we illustrate how 2 can be expressed in array form, whereas in section 3 we review the standard POD-DEIM model reduction strategy. In section 4 we extend POD-DEIM to the multilinear setting and illustrate how it can be applied to systems of array-valued ODEs in section 5. The efficiency of the new procedure is illustrated by numerical experiments in section 6 and our conclusions are formalized in section 7.

Notation. Scalar quantities are indicated by lower case letters and vectors are denoted by bold face lower case letters. Matrices are given by bold face upper case letters, whereas tensors are given by bold face, curly upper case letters and operators by standard curly upper case letters. \mathbf{I}_n denotes the $n \times n$ identity matrix. For a matrix \mathbf{M} , $\|\mathbf{M}\|$ denotes the matrix norm induced by the Euclidean vector norm, and $\|\mathbf{M}\|_F$ is the Frobenius norm. Furthermore, all reduced dimensional quantities are emphasized with a $\hat{\cdot}$.

For a third-order tensor $\mathcal{T} \in \mathbb{R}^{n_1 \times n_2 \times n_3}$, the unfolding along the third mode is given by (see e.g., [29])

$$\mathcal{T}_{(3)} = (\mathbf{T}_1, \mathbf{T}_2, \dots, \mathbf{T}_{n_2}),$$

where $\mathcal{T}_{(3)}$ is a matrix in $\mathbb{R}^{n_3 \times n_1 n_2}$, and $\mathbf{T}_i \in \mathbb{R}^{n_3 \times n_1}$, $i = 1, 2, \dots, n_2$ is called a lateral slice. The multiplication of a tensor by a matrix, along a specific mode is done via the m -mode product, which, for a tensor $\mathcal{T} \in \mathbb{R}^{n_1 \times n_2 \times n_3}$ and a matrix $\mathbf{M} \in \mathbb{R}^{n \times n_m}$, we express as

$$\mathcal{Q} = \mathcal{T} \times_m \mathbf{M} \iff \mathcal{Q}_{(m)} = \mathbf{M} \mathcal{T}_{(m)}.$$

The Kronecker product of two matrices $\mathbf{M} \in \mathbb{R}^{m_1 \times m_2}$ and $\mathbf{N} \in \mathbb{R}^{n_1 \times n_2}$ is defined as

$$\mathbf{M} \otimes \mathbf{N} = \begin{pmatrix} M_{1,1}\mathbf{N} & \cdots & M_{1,m_2}\mathbf{N} \\ \vdots & \ddots & \vdots \\ M_{m_1,1}\mathbf{N} & \cdots & M_{m_1,m_2}\mathbf{N} \end{pmatrix} \in \mathbb{R}^{m_1 n_1 \times m_2 n_2},$$

and the $\text{vec}(\cdot)$ operator maps the entries of a matrix, into a long vector, by stacking the columns of the matrix one after the other. The vectorization operator is applied to a third order tensor, via the first mode unfolding. Moreover, we will often make use of the property

$$(\mathbf{M} \otimes \mathbf{N})\text{vec}(\mathbf{X}) = \text{vec}(\mathbf{N}\mathbf{X}\mathbf{M}^\top). \quad (3)$$

As a result, if $\mathcal{X} \in \mathbb{R}^{n_1 \times n_2 \times n_3}$, and $\mathbf{X} = \mathcal{X}_{(3)}^\top$, then

$$(\mathbf{L} \otimes \mathbf{M} \otimes \mathbf{N}) \text{vec}(\mathcal{X}) = \text{vec}((\mathbf{M} \otimes \mathbf{N}) \mathbf{X} \mathbf{L}^\top). \quad (4)$$

More properties used in the sequel are (see, e.g., [19]): (i) $(\mathbf{M} \otimes \mathbf{N})^\top = \mathbf{M}^\top \otimes \mathbf{N}^\top$; (ii) $(\mathbf{M}_1 \otimes \mathbf{N}_1)(\mathbf{M}_2 \otimes \mathbf{N}_2) = (\mathbf{M}_1 \mathbf{M}_2 \otimes \mathbf{N}_1 \mathbf{N}_2)$; (iii) $\|\mathbf{M} \otimes \mathbf{N}\|_2 = \|\mathbf{M}\|_2 \|\mathbf{N}\|_2$; and (iv) $(\mathbf{M} \otimes \mathbf{N})^{-1} = \mathbf{M}^{-1} \otimes \mathbf{N}^{-1}$, where property (iv) holds if and only if both \mathbf{M} and \mathbf{N} are invertible.

All reported experiments were performed using MATLAB 9.9 (R2020b) ([35]) on a MacBook Pro with 8-GB memory and a 2.3-GHz Intel core i5 processor.

2. Matrix and tensor-based discretization of 1. In this section we illustrate that under certain hypotheses, the discrete system 2 can be expressed in terms of multilinear arrays; see e.g., [47, 12, 40]. To this end, suppose that $\mathcal{L}_1, \dots, \mathcal{L}_g$ are second order differential operators with separable coefficients, such as the Laplace operator. Then, if \mathcal{L}_i is discretized by means of a tensor basis, such as finite differences on parallelepipedal domains and certain spectral methods, the physical domain can be mapped to a reference hypercubic domain $\Omega = [a_1, b_1] \times \dots \times [a_d, b_d]$. Hence, it holds that¹ (see e.g., [40])

$$\mathbf{L}_i = \sum_{m=1}^d \mathbf{I}_{n_d} \otimes \dots \otimes \mathbf{A}_{mi} \otimes \dots \otimes \mathbf{I}_{n_1} \in \mathbb{R}^{N \times N},$$

and

$$\mathbf{D}_i = \sum_{m=1}^d \mathbf{I}_{n_d} \otimes \dots \otimes \mathbf{B}_{mi} \otimes \dots \otimes \mathbf{I}_{n_1} \in \mathbb{R}^{N \times N},$$

where $\mathbf{A}_{mi} \in \mathbb{R}^{n_m \times n_m}$ and $\mathbf{B}_{mi} \in \mathbb{R}^{n_m \times n_m}$ contain the approximation of the second and first derivatives respectively in the x_m direction, for $i = 1, 2, \dots, g$. The vectors $\mathbf{u}_i(t) \in \mathbb{R}^N$ from 2 then represent the vectorization of the elements of a tensor $\mathbf{U}_i(t) \in \mathbb{R}^{n_1 \times \dots \times n_d}$, such that $\mathbf{u}_i(t) = \text{vec}(\mathbf{U}_i(t))$, $\mathbf{L}_i \mathbf{u}_i = \text{vec}(\mathcal{A}_i(\mathbf{U}_i))$ and $\mathbf{D}_i \mathbf{u}_i = \text{vec}(\mathcal{D}_i(\mathbf{U}_i))$, where²

$$\mathcal{A}_i(\mathbf{U}_i) := \sum_{m=1}^d \mathbf{U}_i \times_m \mathbf{A}_{mi} \quad \text{and} \quad \mathcal{D}_i(\mathbf{U}_i) := \sum_{m=1}^d \mathbf{U}_i \times_m \mathbf{B}_{mi}. \quad (5)$$

Moreover, if the function $\mathcal{F}_i : \mathbb{R}^{n_1 \times \dots \times n_d} \times \dots \times \mathbb{R}^{n_1 \times \dots \times n_d} \times [0, t_f] \rightarrow \mathbb{R}^{n_1 \times \dots \times n_d}$ represents the function f_i evaluated at the entries of the arrays $\{\mathbf{U}_i\}_{i=1}^g$ and $\mathcal{D}_i(\mathbf{U}_i)$, then it holds that $\mathbf{f}_i(\mathbf{D}_i \mathbf{u}_i, \mathbf{u}_1, \dots, \mathbf{u}_g, t) = \text{vec}(\mathcal{F}_i(\mathcal{D}_i(\mathbf{U}_i), \mathbf{U}_1, \dots, \mathbf{U}_g, t))$, and 2 can be written in the form

$$\begin{cases} \dot{\mathbf{u}}_1 &= \mathcal{A}_1(\mathbf{U}_1) + \mathcal{F}_1(\mathcal{D}_1(\mathbf{U}_1), \mathbf{U}_1, \mathbf{U}_2, \dots, \mathbf{U}_g, t) \\ &\vdots \\ \dot{\mathbf{u}}_g &= \mathcal{A}_g(\mathbf{U}_g) + \mathcal{F}_g(\mathcal{D}_g(\mathbf{U}_g), \mathbf{U}_1, \mathbf{U}_2, \dots, \mathbf{U}_g, t), \end{cases} \quad (6)$$

with suitable initial conditions. The boundary conditions are contained in the matrices \mathbf{A}_{mi} and \mathbf{B}_{mi} , $i = 1, \dots, g$, $m = 1, \dots, d$; see e.g., [12, 40].

¹We display the discretized Laplace operator, but more general operators can also be treated; see, e.g. [47, Section 3].

²For the case $d = 2$, 5 are Sylvester operators of the form $\mathbf{A}_{1i} \mathbf{U}_i + \mathbf{U}_i \mathbf{A}_{2i}^\top$ and $\mathbf{B}_{1i} \mathbf{U}_i + \mathbf{U}_i \mathbf{B}_{2i}^\top$ respectively [47].

To simplify the presentation, we will consider the case where $n_1 = \dots = n_d = n$ in the sequel, so that $N = n^d$. The extension to the more general case where $n_1 \neq \dots \neq n_d$ is, however, possible.

3. Review of POD-DEIM. In this section we review the standard POD-DEIM method and its application to the dynamical system 2, with $g = 1$ and a nonlinear function independent of the gradient. We aim to reduce the dimension and complexity of a system of ODEs of the form

$$\dot{\mathbf{u}}(t) = \mathbf{L}\mathbf{u}(t) + \mathbf{f}(\mathbf{u}, t), \quad \mathbf{u}(0) = \mathbf{u}_0, \quad (7)$$

with $\mathbf{u}(t) \in \mathbb{R}^N$. Commonly POD is used to reduce the dimension of the state space by projecting onto a subspace of dimension $k \ll N$. In particular, given a set of n_s trajectories (commonly known as snapshots) of the solution $\{\mathbf{u}(t_j)\}_{j=1}^{n_s}$, the POD basis is determined as the best rank k approximation in the 2-norm of the space of snapshots. In particular, for

$$\mathbf{S} = [\mathbf{u}(t_1), \dots, \mathbf{u}(t_{n_s})] \in \mathbb{R}^{N \times n_s},$$

the POD basis $\{\mathbf{v}_1, \dots, \mathbf{v}_k\}$ is determined as the first k dominant left singular vectors of \mathbf{S} . Therefore, if $\mathbf{V} = [\mathbf{v}_1, \dots, \mathbf{v}_k] \in \mathbb{R}^{N \times k}$, then we determine an approximation to $\mathbf{u}(t)$ as $\mathbf{u}(t) \approx \mathbf{V}\hat{\mathbf{u}}(t)$, where $\hat{\mathbf{u}}(t) \in \mathbb{R}^k$ is determined as the solution of the reduced problem

$$\dot{\hat{\mathbf{u}}}(t) = \hat{\mathbf{L}}\hat{\mathbf{u}}(t) + \hat{\mathbf{f}}(\hat{\mathbf{u}}, t), \quad \hat{\mathbf{u}}(0) = \mathbf{V}^\top \mathbf{u}_0, \quad (8)$$

with $\hat{\mathbf{L}} = \mathbf{V}^\top \mathbf{L}\mathbf{V}$ and $\hat{\mathbf{f}}(\hat{\mathbf{u}}, t) = \mathbf{V}^\top \mathbf{f}(\mathbf{V}\hat{\mathbf{u}}, t)$. By definition, $\hat{\mathbf{f}}(\hat{\mathbf{u}}, t)$ first needs to be evaluated in full dimension, that is at the entries of $\mathbf{V}\hat{\mathbf{u}}(t) \in \mathbb{R}^N$, before projection onto the low-dimensional subspace. Hence, the overall cost of evaluating 8 still depends on the full dimension N . One way to treat this bottleneck is through DEIM [8].

DEIM is used to interpolate a nonlinear function on the columns of an empirical basis. In particular if we consider a set of snapshots of the nonlinear function $\{\mathbf{f}(\mathbf{u}, t_i)\}_{i=1}^{n_s}$, then the DEIM basis $\{\phi_1, \dots, \phi_p\}$ is determined as the first p left singular vectors of the matrix

$$\mathbf{N} = [\mathbf{f}(\mathbf{u}, t_1), \dots, \mathbf{f}(\mathbf{u}, t_{n_s})] \in \mathbb{R}^{N \times n_s}.$$

Then, if we set $\Phi = [\phi_1, \dots, \phi_p] \in \mathbb{R}^{N \times p}$ and consider $\mathbf{P} = [\mathbf{e}_{\rho_1}, \dots, \mathbf{e}_{\rho_p}] \in \mathbb{R}^{N \times p}$ as a subset of columns of the $N \times N$ identity matrix, then the DEIM approximation of the nonlinear function is written as

$$\mathbf{f}(\mathbf{u}, t) \approx \Phi (\mathbf{P}^\top \Phi)^{-1} \mathbf{P}^\top \mathbf{f}(\mathbf{u}, t). \quad (9)$$

The interpolation indices $\{\rho_1, \dots, \rho_p\}$ can be determined either in a greedy fashion [8], or through the pivoted QR decomposition of Φ^\top [14]. In the sequel we will make use of the latter algorithm and we will refer to it as **q-deim**. The approximation 9 is particularly advantageous when the function \mathbf{f} is evaluated elementwise at the entries of \mathbf{u} . In this case it holds that $\mathbf{P}^\top \mathbf{f}(\mathbf{u}, t) = \mathbf{f}(\mathbf{P}^\top \mathbf{u}, t)$, and hence \mathbf{f} only needs to be evaluated at p entries.

To complete the reduction of 8 to be independent of N , we therefore approximate $\hat{\mathbf{f}}$ by 9, so that

$$\hat{\mathbf{f}}(\hat{\mathbf{u}}, t) \approx \mathbf{V}^\top \Phi (\mathbf{P}^\top \Phi)^{-1} \mathbf{f}(\mathbf{P}^\top \mathbf{V}\hat{\mathbf{u}}, t). \quad (10)$$

In what follows we illustrate how the POD-DEIM method can be extended to the multilinear setting.

4. POD-DEIM in the multilinear setting. In this section we extend POD-DEIM to the matrix and tensor setting. We illustrate the procedure for systems of the form 6 with $g = 1$ and a gradient-independent nonlinearity. The extension to the case of general g is presented later in the paper. In particular, we want to approximate the solution $\mathbf{U}(t) \in \mathbb{R}^{n \times \dots \times n}$, for $t \in [0, t_f]$, of the equation

$$\dot{\mathbf{U}} = \mathcal{A}(\mathbf{U}) + \mathcal{F}(\mathbf{U}, t), \quad \mathbf{U}(0) = \mathbf{U}_0, \quad (11)$$

by constructing d low-dimensional basis matrices (one for each spatial mode $m = 1, \dots, d$) $\mathbf{V}_m \in \mathbb{R}^{n \times k_m}$, with $k_m \ll n$, to approximate $\mathbf{U}(t)$ in low dimension, for all $t \in [0, t_f]$. To this end, given a set of snapshots $\{\mathbf{U}(t_j)\}_{j=1}^{n_s}$ with $\mathbf{U}(t_j) \in \mathbb{R}^{n \times \dots \times n}$, we define $\mathcal{S} \in \mathbb{R}^{n \times \dots \times n \times n_s}$ as a snapshot tensor³ of order $d+1$ containing a collection of all the snapshots. In the well known case where the snapshots are vectors, this operation corresponds to collecting the vector snapshots into a *snapshot matrix*. Instead, we are dealing with snapshots of higher dimension, which results in the definition of a *snapshot tensor*.

Then, given \mathcal{S} , each matrix \mathbf{V}_m is constructed in order to approximate the left range space of the matrix

$$\mathcal{S}_{(m)} = (\mathbf{U}_{(m)}(t_1), \dots, \mathbf{U}_{(m)}(t_{n_s})) \in \mathbb{R}^{n \times n^{d n_s}}, \quad \text{for } m = 1, \dots, d,$$

where m represents the mode along which the tensor is unfolded. Forming or storing the matrix $\mathcal{S}_{(m)}$ is too computationally demanding, even for moderate n and n_s . Instead, the approximation spaces are updated one snapshot at a time.

To this end, we determine the sequentially truncated higher order SVD⁴ (STHOSVD) [52] of each snapshot $\mathbf{U}(t_j)$, so that $\mathbf{U}(t_j) \approx \mathcal{C}(t_j) \times_{m=1}^d \tilde{\mathbf{V}}_m^{(j)}$, where $\tilde{\mathbf{V}}_m^{(j)}$ contains the dominant left singular vectors of $\mathbf{U}_{(m)}(t_j)$, truncated with respect to the tolerance τ . Furthermore, $\mathcal{C}(t_j)$ is the core tensor related to the STHOSVD of $\mathbf{U}(t_j)$, and is generally defined as $\mathcal{C}(t_j) = \mathbf{U}(t_j) \times_{m=1}^d (\tilde{\mathbf{V}}_m^{(j)})^\top$. Note, however, that in our procedure it is not necessary to explicitly compute the core tensors $\mathcal{C}(t_j)$, since only the matrices $\tilde{\mathbf{V}}_m^{(j)}$ are required. More precisely, the approximation space in each mode is updated by orthogonalizing $\tilde{\mathbf{V}}_m^{(j)}$ with respect to the previous basis vectors in that mode, and pruning any redundant information, with respect to τ , to update \mathbf{V}_m . Through this procedure each snapshot can be discarded after it has been processed. We will refer to this as the higher order POD (HO-POD) approximation. We call this a higher order approximation, since the standard POD projection is only a one-sided approximation, whereas this procedure is two-sided or three-sided for $d = 2$ and $d = 3$ respectively.

This type of approximation can also be interpreted as a Tucker _{d} decomposition (see e.g., [29, Section 4]) of the snapshot tensor $\mathcal{S} \in \mathbb{R}^{n \times \dots \times n \times n_s}$ of the form

$$\mathcal{S} \approx \hat{\mathcal{S}} \times_1 \mathbf{V}_1 \times_2 \dots \times_d \mathbf{V}_d \times_{d+1} \mathbf{I}_{n_s}, \quad \hat{\mathcal{S}} \in \mathbb{R}^{k_1 \times \dots \times k_d \times n_s},$$

since the principal components of each of the first d modes are analyzed. Nevertheless, instead of determining the core tensor $\hat{\mathcal{S}}$, which contains a collection of low-dimensional approximations to all the given snapshots, we aim to use the basis matrices to approximate the solution of 11 at time instances other than the ones considered for the snapshots.

³We emphasize that this large dimensional tensor will never be explicitly formed or stored.

⁴For the case $d = 2$, however, we just use the standard MATLAB SVD function.

More precisely, we look for a approximation to the solution of [11](#) of the form $\mathbf{u}(t) \approx \tilde{\mathbf{u}}(t) := \hat{\mathbf{u}}(t) \times_{m=1}^d \mathbf{V}_m$, where $\hat{\mathbf{u}}(t) \in \mathbb{R}^{k_1 \times \dots \times k_d}$ ($k_m \ll n$) satisfies the low-dimensional equation

$$\dot{\hat{\mathbf{u}}} = \hat{\mathcal{A}}(\hat{\mathbf{u}}) + \hat{\mathcal{F}}(\hat{\mathbf{u}}, t), \quad \hat{\mathbf{u}}(0) = \hat{\mathbf{u}}_0, \quad (12)$$

where

$$\hat{\mathcal{A}}(\hat{\mathbf{u}}) := \sum_{m=1}^d \hat{\mathbf{u}} \times_m \hat{\mathbf{A}}_m, \quad \hat{\mathbf{A}}_m = \mathbf{V}_m^\top \mathbf{A}_m \mathbf{V}_m, \quad \hat{\mathbf{u}}(0) = \mathbf{u}_0 \times_{m=1}^d \mathbf{V}_m^\top \quad (13)$$

and

$$\hat{\mathcal{F}}(\hat{\mathbf{u}}, t) = \mathcal{F}(\tilde{\mathbf{u}}(t), t) \times_{m=1}^d \mathbf{V}_m^\top. \quad (14)$$

For the time discretization of [12](#), several alternatives can be considered, however it is well known that these type of semilinear equations are typically characterized by a stiff linear term and a nonstiff nonlinear term; see e.g., [\[49\]](#). That is, explicit methods will require unrealistically small timesteps to ensure stability in the linear term, whereas fully implicit schemes require the application of an expensive iterative nonlinear solver at each timestep. Instead, a good compromise is reached through semi-implicit (also called implicit-explicit) schemes, where the linear term is treated implicitly and the nonlinear term explicitly [\[24, chapter IV.3\]](#). To this end, we consider a second order implicit-explicit scheme, also known as IMEX 2–SBDF; see e.g., [\[12, 2\]](#). Therefore, if $\hat{\mathbf{u}}^{(j)}$ is an approximation of $\hat{\mathbf{u}}(t_j)$, then the linear system

$$(3\hat{\mathcal{I}} - 2\Delta t \hat{\mathcal{A}}) \hat{\mathbf{u}}^{(j)} = \hat{\mathcal{G}}(\hat{\mathbf{u}}^{(j-1)}, \hat{\mathbf{u}}^{(j-2)}) \quad (15)$$

needs to be solved for each t_j , where

$$\hat{\mathcal{G}}(\hat{\mathbf{u}}^{(j-1)}, \hat{\mathbf{u}}^{(j-2)}) = 4\hat{\mathbf{u}}^{(j-1)} - \hat{\mathbf{u}}^{(j-2)} + 2\Delta t \left(2\hat{\mathcal{F}}(\hat{\mathbf{u}}^{(j-1)}, t_{j-1}) - \hat{\mathcal{F}}(\hat{\mathbf{u}}^{(j-2)}, t_{j-2}) \right),$$

and $\hat{\mathcal{I}} : \mathbb{R}^{k_1 \times \dots \times k_d} \rightarrow \mathbb{R}^{k_1 \times \dots \times k_d}$ is the identity operator in the reduced dimension. To initiate the procedure, $\hat{\mathbf{u}}^{(1)}$ can be determined by a semi-implicit Euler scheme from the known array $\hat{\mathbf{u}}^{(0)}$. In what follows we discuss how [15](#) is solved for $d = 2, 3$.

4.1. The solution of the linear system [15](#). The solution of [15](#) is not trivial, especially when $d = 3$, given that the matrices $\hat{\mathbf{A}}_m$, for $m = 1, \dots, d$ are necessarily dense due to the projection. When $d = 2$, it holds that $\hat{\mathbf{u}}^{(j)} = \hat{\mathbf{U}}^{(j)} \in \mathbb{R}^{k_1 \times k_2}$, and $\hat{\mathcal{A}}$ is a Sylvester operator [\[47\]](#), so that [15](#) is equivalent to the Sylvester equation (see e.g., [\[12\]](#))

$$(3\mathbf{I}_{k_1} - 2\Delta t \hat{\mathbf{A}}_1) \hat{\mathbf{U}}^{(j)} + \hat{\mathbf{U}}^{(j)} (-2\Delta t \hat{\mathbf{A}}_2^\top) = \hat{\mathcal{G}}(\hat{\mathbf{U}}^{(j-1)}, \hat{\mathbf{U}}^{(j-2)}).$$

Details on how to solve the Sylvester equation can be found in [\[47\]](#). In our experiments we make use of the built-in MATLAB function `lyap`.

For the case $d = 3$, a direct method designed specifically for dense third order tensor linear systems has recently been introduced in [\[46\]](#) for tensors with a rank-one right hand side. Here we illustrate how this method can be applied to solve the linear system [15](#), accounting for a right hand side with rank greater than one. To ease the readability, we drop the superscript (j) for the description of the inner solver, when it is clear from the context.

By definition, when $d = 3$, the left hand side of 15 can be vectorized as

$$\left(\mathbf{I}_{k_3} \otimes 3\mathbf{I}_{k_2} \otimes \mathbf{I}_{k_1} - \mathbf{I}_{k_3} \otimes \mathbf{I}_{k_2} \otimes 2\Delta t \widehat{\mathbf{A}}_1 - \mathbf{I}_{k_3} \otimes 2\Delta t \widehat{\mathbf{A}}_2 \otimes \mathbf{I}_{k_1} - 2\Delta t \widehat{\mathbf{A}}_3 \otimes \mathbf{I}_{k_2} \otimes \mathbf{I}_{k_1} \right) \text{vec} \left(\widehat{\mathbf{u}} \right).$$

Therefore, if we let $\widehat{\mathbf{X}} = \widehat{\mathbf{u}}_{(3)}^\top \in \mathbb{R}^{k_1 k_2 \times k_3}$, then by the use of property 4, 15 can be recast into the Sylvester equation

$$\left(3\mathbf{I}_{k_2} \otimes \mathbf{I}_{k_1} - \mathbf{I}_{k_2} \otimes 2\Delta t \widehat{\mathbf{A}}_1 - 2\Delta t \widehat{\mathbf{A}}_2 \otimes \mathbf{I}_{k_1} \right) \widehat{\mathbf{X}} + \widehat{\mathbf{X}} \left(-2\Delta t \widehat{\mathbf{A}}_3^\top \right) = \widehat{\mathbf{G}}. \quad (16)$$

Here $\widehat{\mathbf{G}} = \widehat{\mathcal{G}}(\widehat{\mathbf{X}}^{(j-1)}, \widehat{\mathbf{X}}^{(j-2)}) \in \mathbb{R}^{k_1 k_2 \times k_3}$. Due to the large left dimension of this Sylvester equation, solving this directly is still not feasible. Instead, as is shown in [46], it is possible to solve a sequence of much smaller Sylvester equations. To this end, let $\widehat{\mathbf{A}}_3^\top = \mathbf{Q}\mathbf{R}\mathbf{Q}^\top$ be the Schur decomposition of $\widehat{\mathbf{A}}_3^\top$. Then, if $\widehat{\mathbf{Y}} = \widehat{\mathbf{X}}\mathbf{Q}$, it holds that

$$\left(3\mathbf{I}_{k_2} \otimes \mathbf{I}_{k_1} - \mathbf{I}_{k_2} \otimes 2\Delta t \widehat{\mathbf{A}}_1 - 2\Delta t \widehat{\mathbf{A}}_2 \otimes \mathbf{I}_{k_1} \right) \widehat{\mathbf{Y}} + \widehat{\mathbf{Y}} \left(-2\Delta t \mathbf{R} \right) = \widehat{\mathbf{G}}\mathbf{Q}, \quad (17)$$

where $\mathbf{R} \in \mathbb{R}^{k_3 \times k_3}$ is block upper triangular. Therefore, by following the ideas of [46] and repeatedly using the property 3, the solution of 15, unfolded in the third mode, is given by

$$\widehat{\mathbf{u}}_{(3)} = (\widehat{\mathbf{Y}}\mathbf{Q}^\top)^\top = \mathbf{Q} \left(\text{vec}(\mathbf{Z}_1)^\top; \dots; \text{vec}(\mathbf{Z}_{k_3})^\top \right) \in \mathbb{R}^{k_3 \times k_1 k_2}.$$

Here, $\mathbf{Z}_h \in \mathbb{R}^{k_1 \times k_2}$ ($h = 1, 2, \dots, k_3$) solves the smaller Sylvester equation

$$\left((3 - 2\Delta t \mathbf{R}_{h,h}) \mathbf{I}_{k_1} - 2\Delta t \widehat{\mathbf{A}}_1 \right) \mathbf{Z}_h + \mathbf{Z}_h \left(-2\Delta t \widehat{\mathbf{A}}_2^\top \right) = \mathbf{H}_h + 2\Delta t \mathbf{J}_{h-1},$$

where $\widehat{\mathbf{G}}\mathbf{Q} = \mathbf{H} = (\text{vec}(\mathbf{H}_1), \dots, \text{vec}(\mathbf{H}_{k_3})) \in \mathbb{R}^{k_1 k_2 \times k_3}$, and $\mathbf{J}_{h-1} \in \mathbb{R}^{k_1 \times k_2}$ is the matricization of

$$\text{vec}(\mathbf{J}_{h-1}) = (\text{vec}(\mathbf{Z}_1), \dots, \text{vec}(\mathbf{Z}_{h-1})) \mathbf{R}_{h,1:h-1}. \quad (18)$$

In the special case where all coefficient matrices are symmetric and positive definite, the procedure can be even further accelerated; see [46] for further details. We refer to this inner solver as the T3-SYLV solver.

4.2. Interpolation of the nonlinear function by HO-DEIM. To determine the right-hand side $\widehat{\mathcal{G}}(\widehat{\mathbf{u}}^{(j-1)}, \widehat{\mathbf{u}}^{(j-2)})$ at each t_j , it is required to evaluate the nonlinear function in full dimension, as per the definition of $\widehat{\mathcal{F}}(\widehat{\mathbf{u}}, t)$. Instead, we interpolate the nonlinear function through a higher order DEIM. Consider the d low-dimensional orthonormal matrices $\Phi_m \in \mathbb{R}^{n \times p_m}$, with $p_m \ll n$, determined as the output of HO-POD of the set of nonlinear snapshots $\{\mathcal{F}(\mathbf{u}(t_j), t_j)\}_{j=1}^{n_s}$, for $m = 1, 2, \dots, d$. Furthermore, consider the d selection matrices $\mathbf{P}_m \in \mathbb{R}^{n \times p_m}$, given as the output of q-deim with input Φ_m^\top , for $m = 1, 2, \dots, d$. The HO-DEIM approximation of 14 is then given by

$$\widehat{\mathcal{F}}(\widehat{\mathbf{u}}, t) \approx \mathcal{F}(\widetilde{\mathbf{u}}, t) \times_{m=1}^d \mathbf{V}_m^\top \Phi_m (\mathbf{P}_m^\top \Phi_m)^{-1} \mathbf{P}_m^\top. \quad (19)$$

If \mathcal{F} is evaluated elementwise at the components of $\widetilde{\mathbf{u}}$, then it holds that

$$\widehat{\mathcal{F}}(\widehat{\mathbf{u}}, t) := \mathcal{F}(\widetilde{\mathbf{u}}, t) \times_{m=1}^d \mathbf{P}_m^\top = \mathcal{F}(\widetilde{\mathbf{u}} \times_{m=1}^d \mathbf{P}_m^\top, t). \quad (20)$$

Notice that \mathcal{F} is then evaluated at $p_1 p_2 \cdots p_d \ll n^d$ entries. Next we remark on a potential strategy for further reducing the online cost of the procedure. This is, however, not considered in our implementations.

Remark 1. For certain nonlinear functions, the evaluation of $p_1 p_2 \cdots p_d$ entries online may not be feasible. One possibility that can be considered is to further approximate the HO-DEIM reduced nonlinear function by a matrix-DEIM (MDEIM) type of interpolation (see e.g., [7, 38]). More precisely, if we consider the HO-DEIM approximations 19 and 20 then the snapshot matrix $\mathfrak{N} = [\mathbf{f}(t_1), \dots, \mathbf{f}(t_{n_s})] \in \mathbb{R}^{p_1 \cdots p_d \times n_s}$, can be considered, where

$$\mathbf{f}(t_j) = \text{vec} \left(\widehat{\mathcal{F}(\tilde{\mathbf{u}}, t_j)} \times_{m=1}^d (\mathbf{P}_m^\top \Phi_m)^{-1} \right) \in \mathbb{R}^{p_1 \cdots p_d}.$$

If we define $\mathcal{M}_q \in \mathbb{R}^{p_1 \times \cdots \times p_d}$ as the tensorization of the q th column of $\mathfrak{M} \in \mathbb{R}^{p_1 \cdots p_d \times \mathfrak{p}}$ - the matrix of dominant left singular vectors of \mathfrak{N} - then

$$\widehat{\mathcal{F}}(\tilde{\mathbf{u}}, t) \approx \sum_{q=1}^{\mathfrak{p}} c_q \mathcal{M}_q \times_{m=1}^d \mathbf{V}_m^\top \Phi_m, \quad c_q = \left[(\mathfrak{P}^\top \mathfrak{M})^{-1} \mathbf{f} \left(\mathfrak{P}^\top \text{vec} \left(\tilde{\mathbf{u}} \times_{m=1}^d \mathbf{P}_m^\top \right), t \right) \right]_q,$$

where the columns of $\mathfrak{P} \in \mathbb{R}^{p_1 \cdots p_d \times \mathfrak{p}}$ are related to the \mathbf{q} -deim interpolation indices of the matrix \mathfrak{M} . Note that the nonlinear function is now evaluated at $\mathfrak{p} \ll p_1 \cdots p_d$ entries, even though no vectors of length N need to be stored. This type of approximation has a couple of drawbacks, however. Firstly, to determine the snapshots $\mathbf{f}(t_j)$, another (far cheaper) offline phase will be required. Moreover, potential structural properties such as symmetries, which are preserved by the approximation 19, may be destroyed by the vectorization; see also the discussion in the companion manuscript [28, Section 4].

We next provide an error bound for the HO-DEIM approximation 19, where we recall that the matrices Φ_m , for $m = 1, 2, \dots, d$ all have orthonormal columns. This bound is a direct extension to the array setting of [8, Lemma 3.2]. A similar result can be found in [28] for $d = 2$.

Proposition 1. Let $\mathbf{Q}_m = \Phi_m (\mathbf{P}_m^\top \Phi_m)^{-1} \mathbf{P}_m^\top$, and consider an arbitrary tensor $\mathcal{F} \in \mathbb{R}^{n \times \cdots \times n}$, so that

$$\tilde{\mathcal{F}} = \mathcal{F} \times_{m=1}^d \Phi_m (\mathbf{P}_m^\top \Phi_m)^{-1} \mathbf{P}_m^\top = \mathcal{F} \times_{m=1}^d \mathbf{Q}_m.$$

Then,

$$\|\mathcal{F} - \tilde{\mathcal{F}}\|_F \leq c_1 c_2 \cdots c_d \|\mathcal{F} - \mathcal{F} \times_{m=1}^d \Phi_m \Phi_m^\top\|_F \quad (21)$$

where $c_m = \|(\mathbf{P}_m^\top \Phi_m)^{-1}\|_2$, for $m = 1, \dots, d$.

Proof. Let $\mathbf{f} = \text{vec}(\mathcal{F}) \in \mathbb{R}^N$. Then, by the properties of the Kronecker product

$$\begin{aligned} \|\mathcal{F} - \tilde{\mathcal{F}}\|_F &= \|\text{vec}(\mathcal{F}) - \text{vec}(\tilde{\mathcal{F}})\|_2 = \|\mathbf{f} - (\mathbf{Q}_d \otimes \cdots \otimes \mathbf{Q}_1) \mathbf{f}\|_2 \\ &= \left\| \mathbf{f} - (\Phi_d \otimes \cdots \otimes \Phi_1) \left((\mathbf{P}_d \otimes \cdots \otimes \mathbf{P}_1)^\top (\Phi_d \otimes \cdots \otimes \Phi_1) \right)^{-1} (\mathbf{P}_d \otimes \cdots \otimes \mathbf{P}_1)^\top \mathbf{f} \right\|_2 \end{aligned}$$

Therefore, by [8, Lemma 3.2],

$$\begin{aligned} \|\mathcal{F} - \tilde{\mathcal{F}}\|_F &\leq \left\| \left((\mathbf{P}_d \otimes \cdots \otimes \mathbf{P}_1)^\top (\Phi_d \otimes \cdots \otimes \Phi_1) \right)^{-1} \right\|_2 \left\| \mathbf{f} - (\Phi_d \otimes \cdots \otimes \Phi_1) (\Phi_d \otimes \cdots \otimes \Phi_1)^\top \mathbf{f} \right\|_2 \\ &= \left\| (\mathbf{P}_d^\top \Phi_d)^{-1} \right\|_2 \cdots \left\| (\mathbf{P}_2^\top \Phi_2)^{-1} \right\|_2 \left\| (\mathbf{P}_1^\top \Phi_1)^{-1} \right\|_2 \left\| \mathcal{F} - \mathcal{F} \times_{m=1}^d \Phi_m \Phi_m^\top \right\|_F. \end{aligned}$$

□

The accuracy of the HO-DEIM approximation therefore depends on the contraction coefficients c_m , which are minimized by the use of **q-deim**; see, e.g., [14]. Furthermore it depends on the accuracy of the HO-POD bases, given by the term $\left\| \mathcal{F} - \mathcal{F} \times_{m=1}^d \Phi_m \Phi_m^\top \right\|_F$.

The full offline/online HO-POD-DEIM reduction procedure for reducing tensor-valued ODEs is presented below in algorithm HO-POD-DEIM for the case $d = 3$. In what follows, we illustrate how the discussed higher-order POD-DEIM order

Algorithm HO-POD-DEIM for Tensor ODEs, $d = 3$

Given: Coefficient matrices of **11** and function $\mathcal{F} : \mathbb{R}^{n \times \cdots \times n} \times [0, t_f] \rightarrow \mathbb{R}^{n \times \cdots \times n}$

Offline:

1. For each $j = 1, 2, \dots, n_s$
 - (i) Iteratively update $\{\mathbf{V}_m\}_{m=1}^3$ and $\{\Phi_m\}_{m=1}^3$, for the snapshots $\mathbf{u}(t_j)$ and $\mathcal{F}(\mathbf{u}(t_j), t_j)$ respectively as **11** is integrated in time and discard the snapshots (HO-POD);
2. Compute $\hat{\mathbf{A}}_m$, for $m = 1, 2, 3$ and $\hat{\mathbf{u}}(0)$ from **(13)**;
3. Determine $\{\mathbf{P}_m\}_{m=1}^3$ using **q-deim** (HO-DEIM);
4. Precompute $\{\mathbf{V}_m^\top \Phi_m (\mathbf{P}_m^\top \Phi_m)^{-1}\}_{m=1}^3$ and $\{\mathbf{P}_m^\top \mathbf{V}_m\}_{m=1}^3$;
5. Compute the Schur decomposition $\hat{\mathbf{A}}_3^\top = \mathbf{Q}\mathbf{R}\mathbf{Q}^\top$;

Online:

1. Determine $\hat{\mathbf{u}}^{(1)}$ from $\hat{\mathbf{u}}^{(0)}$;
 2. For each $j = 2, 3, \dots, n_t$
 - (i) Approximate $\hat{\mathcal{F}}(\hat{\mathbf{u}}^{(j-1)}, t_{j-1})$ and $\hat{\mathcal{F}}(\hat{\mathbf{u}}^{(j-2)}, t_{j-2})$ as in **19** and **20** using the matrices computed above, and evaluate $\mathcal{G}(\hat{\mathbf{u}}^{(j-1)}, \hat{\mathbf{u}}^{(j-2)})$;
 - (ii) For each $h = 1, 2, \dots, k_3$:
 - (a) Evaluate \mathbf{J}_{h-1} using **18** and compute $\mathbf{H} = \hat{\mathbf{G}}\mathbf{Q}$;
 - (b) Reshape column h of \mathbf{H} into a $k_1 \times k_2$ matrix to form \mathbf{H}_h ;
 - (c) Solve the Sylvester matrix equation by a direct solver:
$$\left((3 - 2\Delta t \mathbf{R}_{h,h}) \mathbf{I}_k - 2\Delta t \hat{\mathbf{A}} \right) \mathbf{Z}_h + \mathbf{Z}_h \left(-2\Delta t \hat{\mathbf{B}}^\top \right) = \mathbf{H}_h + 2\Delta t \mathbf{J}_{h-1},$$
 - (d) Update $\mathbf{Z} \leftarrow [\mathbf{Z}, \text{vec}(\mathbf{Z}_h)]$;
 - (iii) Evaluate $\hat{\mathbf{u}}_{(3)}^{(j)} = \mathbf{Q}\mathbf{Z}^\top$ and reshape it into a $k_1 \times k_2 \times k_3$ tensor;
 3. Return $\mathbf{V}_1, \mathbf{V}_2, \mathbf{V}_3$ and $\{\hat{\mathbf{u}}_{(3)}^{(j)}\}_{j=1}^{n_t}$, so that $\hat{\mathbf{u}}^{(j)} \times_1 \mathbf{V}_1 \times_2 \mathbf{V}_2 \times_3 \mathbf{V}_3 \approx \mathbf{u}(t_j)$;
-

reduction strategy can be applied to systems of ODEs of the form **6**.

5. Order reduction of systems of array-valued ODEs. Here we illustrate how the HO-POD-DEIM order reduction scheme presented in the previous section can be applied to systems of array-valued ODEs of the form 6. Indeed, consider $d \cdot g$ tall basis matrices $\mathbf{V}_{m,i} \in \mathbb{R}^{n \times k_{mi}}$ with orthonormal columns, for $i = 1, 2, \dots, g$ and $m = 1, 2, \dots, d$, where $k_{mi} \ll n$. That is, we consider d basis matrices for each of the g equations in 6. Approximations to each $\mathbf{u}_i(t)$, for $t \in [0, t_f]$, can then be written as

$$\mathbf{u}_i(t) \approx \tilde{\mathbf{u}}_i(t) = \hat{\mathbf{u}}_i(t) \times_{m=1}^d \mathbf{V}_{m,i}, \quad i = 1, 2, \dots, g.$$

The functions $\hat{\mathbf{u}}_i(t) \in \mathbb{R}^{k_{1i} \times k_{2i} \times \dots \times k_{di}}$ are determined as an approximation to the solution of the reduced, coupled problem

$$\begin{cases} \dot{\hat{\mathbf{u}}}_1 &= \hat{\mathcal{A}}_1(\hat{\mathbf{u}}_1) + \hat{\mathcal{F}}_1(\hat{\mathcal{D}}_1(\hat{\mathbf{u}}_1), \hat{\mathbf{u}}_1, \hat{\mathbf{u}}_2, \dots, \hat{\mathbf{u}}_g, t) \\ &\vdots \\ \dot{\hat{\mathbf{u}}}_g &= \hat{\mathcal{A}}_g(\hat{\mathbf{u}}_g) + \hat{\mathcal{F}}_g(\hat{\mathcal{D}}_g(\hat{\mathbf{u}}_g), \hat{\mathbf{u}}_1, \hat{\mathbf{u}}_2, \dots, \hat{\mathbf{u}}_g, t), \end{cases} \quad (22)$$

where

$$\hat{\mathcal{A}}_i(\hat{\mathbf{u}}_i) := \sum_{m=1}^d \hat{\mathbf{u}}_i \times_m \hat{\mathbf{A}}_{mi}, \quad \hat{\mathbf{A}}_{mi} = \mathbf{V}_{m,i}^\top \mathbf{A}_{mi} \mathbf{V}_{m,i}, \quad \hat{\mathbf{u}}(0) = \mathbf{u}_{i0} \times_{m=1}^d \mathbf{V}_{m,i}^\top \quad (23)$$

and

$$\hat{\mathcal{F}}_i(\hat{\mathcal{D}}_i(\hat{\mathbf{u}}_i), \hat{\mathbf{u}}_1, \dots, \hat{\mathbf{u}}_g, t) = \mathcal{F}_i(\mathcal{D}_i(\tilde{\mathbf{u}}_i), \tilde{\mathbf{u}}_1, \dots, \tilde{\mathbf{u}}_g, t) \times_{m=1}^d \mathbf{V}_{m,i}^\top. \quad (24)$$

We use the HO-POD procedure from the previous section to determine the basis matrices. In particular, given the set of snapshot solutions $\{\mathbf{u}_i(t_j)\}_{j=1}^{n_s}$, the basis matrices $\mathbf{V}_{m,i} \in \mathbb{R}^{n \times k_{mi}}$, $m = 1, 2, \dots, d$, are determined following the HO-POD procedure from section 4, for each $i = 1, 2, \dots, g$.

The reduced order model 22, can also be integrated by means of the IMEX 2 - SBDF scheme for systems. Indeed, the $\hat{\mathbf{u}}_1^{(j)}, \hat{\mathbf{u}}_2^{(j)}, \dots, \hat{\mathbf{u}}_g^{(j)}$ approximations to $\hat{\mathbf{u}}_1(t_j), \hat{\mathbf{u}}_2(t_j), \dots, \hat{\mathbf{u}}_g(t_j)$ are determined by solving the linear systems

$$\begin{cases} (3\hat{\mathcal{I}} - 2\Delta t \hat{\mathcal{A}}_1)(\hat{\mathbf{u}}_1^{(j)}) &= \hat{\mathcal{G}}_1 \left(\{\hat{\mathbf{u}}_i^{(j-1)}\}_{i=1}^g, \{\hat{\mathbf{u}}_i^{(j-2)}\}_{i=1}^g \right) \\ &\vdots \\ (3\hat{\mathcal{I}} - 2\Delta t \hat{\mathcal{A}}_g)(\hat{\mathbf{u}}_g^{(j)}) &= \hat{\mathcal{G}}_g \left(\{\hat{\mathbf{u}}_i^{(j-1)}\}_{i=1}^g, \{\hat{\mathbf{u}}_i^{(j-2)}\}_{i=1}^g \right), \end{cases} \quad (25)$$

at each t_j , where

$$\begin{aligned} \hat{\mathcal{G}}_i \left(\{\hat{\mathbf{u}}_i^{(j-1)}\}_{i=1}^g, \{\hat{\mathbf{u}}_i^{(j-2)}\}_{i=1}^g \right) &= 4\hat{\mathbf{u}}_i^{(j-1)} + 4\Delta t \hat{\mathcal{F}}_i \left(\hat{\mathcal{D}}_i(\hat{\mathbf{u}}_i^{(j-1)}), \hat{\mathbf{u}}_1^{(j-1)}, \dots, \hat{\mathbf{u}}_g^{(j-1)}, t_{j-1} \right) \\ &\quad - \hat{\mathbf{u}}_i^{(j-2)} - 2\Delta t \hat{\mathcal{F}}_i \left(\hat{\mathcal{D}}_i(\hat{\mathbf{u}}_i^{(j-2)}), \hat{\mathbf{u}}_1^{(j-2)}, \dots, \hat{\mathbf{u}}_g^{(j-2)}, t_{j-2} \right). \end{aligned}$$

Each of the g linear systems in 25 can be solved via the procedures set forth in section 4.1 for $d = 2, 3$.

Adjacent to the setting discussed in section 4.2, the nonlinear functions need to be interpolated to avoid evaluating the functions in full dimension at each timestep. To this end, we approximate $\hat{\mathcal{F}}_i(\hat{\mathcal{D}}_i(\hat{\mathbf{u}}_i), \hat{\mathbf{u}}_1, \dots, \hat{\mathbf{u}}_g, t)$ in the space spanned by the columns of the matrices $\Phi_{m,i} \in \mathbb{R}^{n \times p_{mi}}$, $m = 1, 2, \dots, d$, for each $i = 1, 2, \dots, g$,

where $p_{mi} \ll n$. Given the selection matrices $\mathbf{P}_{m,i} \in \mathbb{R}^{n \times p_{mi}}$, $m = 1, 2, \dots, d$, we obtain

$$\widehat{\mathcal{F}}_i(\widehat{\mathcal{D}}_i(\widehat{\mathbf{U}}_i), \widehat{\mathbf{U}}_1, \dots, \widehat{\mathbf{U}}_g, t) \approx \mathcal{F}_i(\mathcal{D}_i(\widetilde{\mathbf{U}}_i), \widetilde{\mathbf{U}}_1, \dots, \widetilde{\mathbf{U}}_g, t) \times_{m=1}^d \mathbf{V}_{m,i}^\top \mathbf{Q}_{m,i}, \quad (26)$$

with the oblique projectors

$$\mathbf{Q}_{m,i} = \Phi_{m,i}(\mathbf{P}_{m,i}^\top \Phi_{m,i})^{-1} \mathbf{P}_{m,i}^\top, \quad \text{for } m = 1, 2, \dots, d \quad \text{and } i = 1, 2, \dots, g.$$

The basis matrices $\Phi_{m,i}$, $m = 1, 2, \dots, d$ are determined via the HO-POD procedure described in section 4, given the set of nonlinear snapshots

$$\{\mathcal{F}_i(\mathcal{D}_i(\mathbf{U}_i(t_j)), \mathbf{U}_1(t_j), \mathbf{U}_2(t_j), \dots, \mathbf{U}_g(t_j), t_j)\}_{j=1}^{n_s}, \quad (27)$$

whereas the selection matrices $\mathbf{P}_{m,i}$ are determined via **q-deim** with inputs $\Phi_{m,i}^\top$ respectively, for each $i = 1, 2, \dots, g$. In this paper we assume that there is a componentwise relationship between the arrays $\mathbf{U}_1(t_j), \mathbf{U}_2(t_j), \dots, \mathbf{U}_g(t_j)$ and the approximation to the gradient $\mathcal{D}_i(\mathbf{U}_i)$ in the nonlinear function \mathcal{F}_i . Therefore, since the matrix $\mathbf{P}_{m,i}$ is merely responsible for selecting rows in the respective modes, it holds that

$$\begin{aligned} \overline{\mathcal{F}_i(\mathcal{D}_i(\widetilde{\mathbf{U}}_i), \widetilde{\mathbf{U}}_1, \dots, \widetilde{\mathbf{U}}_g, t)} &:= \mathcal{F}_i(\mathcal{D}_i(\widetilde{\mathbf{U}}_i), \widetilde{\mathbf{U}}_1, \dots, \widetilde{\mathbf{U}}_g, t) \times_{m=1}^d \mathbf{P}_{m,i}^\top \\ &= \mathcal{F}_i\left(\mathcal{D}_i(\widetilde{\mathbf{U}}_i) \times_{m=1}^d \mathbf{P}_{m,i}^\top, \widetilde{\mathbf{U}}_1 \times_{m=1}^d \mathbf{P}_{m,i}^\top, \dots, \widetilde{\mathbf{U}}_g \times_{m=1}^d \mathbf{P}_{m,i}^\top, t\right). \end{aligned}$$

6. Numerical experiments. In this section we illustrate the efficiency of the discussed methods via benchmark problems from biology and engineering. For all problems, the accuracy of the reduced order model is tested through the average error measure

$$\bar{\varepsilon}(\mathbf{u}) = \frac{1}{n_t} \sum_{j=1}^{n_t} \frac{\|\mathbf{u}^{(j)} - \widetilde{\mathbf{u}}^{(j)}\|_F}{\|\mathbf{u}^{(j)}\|_F}, \quad (28)$$

and the truncation of the singular values is done by monitoring the quality of the approximation in the Frobenius norm. That is, if $\sigma_1 \geq \sigma_2 \geq \dots \geq \sigma_\kappa$ are the singular values of the matrix that needs to be truncated, then the new dimension $\nu \leq \kappa$ is determined as

$$\frac{\sqrt{\sum_{i=\nu+1}^{\kappa} \sigma_i^2}}{\sqrt{\sum_{i=1}^{\kappa} \sigma_i^2}} < \tau. \quad (29)$$

We first illustrate the efficiency with two examples where $d = 2$, after which we investigate the three-dimensional coupled Burgers equation.

Example 1. *The 2D FitzHugh-Nagumo model (FN).* Consider the following classical problem, given in adimensional form,

$$\dot{u}_1 = \delta_1 \Delta u_1 + \Gamma(-u_1^3 + u_1 - u_2), \quad \dot{u}_2 = \delta_2 \Delta u_2 + \Gamma(\beta u_1 - \beta h u_2), \quad (30)$$

where the functions $u_1(x, y, t)$ and $u_2(x, y, t)$ model the densities of two species for $t \in [0, 1]$, and $[x, y] \in [-1, 1]^2$. We refer the reader to, e.g., [16] for a description of the role of the nonnegative coefficients h, β , and Γ . For this example we set

$h = 0.5, \beta = 2.1, \Gamma = 9.65, \delta_1 = 0.01$ and $\delta_2 = 0.1$. Furthermore, homogeneous Neumann boundary conditions are imposed and the initial state is given by

$$\begin{aligned} u_1(x, y, 0) &= (1 - x^2)(1 - y^2) \sin(2\pi x) \cos(2\pi(y + 0.3)) \\ u_2(x, y, 0) &= (1 - x^2)(1 - y^2) e^{-\sin(2\pi(x-0.3)y)}. \end{aligned}$$

This example investigates the efficiency of the reduced order model in terms of accuracy and online CPU time. To this end, the system 30 is discretized with $n = 1200$ spatial nodes in each direction yielding the form 6. Note that this is equivalent to the system 2 with dimension $N = 1\,440\,000$.

In particular, if we let $\mathbf{T} = \text{tridiag}(1, \underline{-2}, 1) + \mathbf{N}$, $\mathbf{T} \in \mathbb{R}^{n \times n}$, where

$$\mathbf{N} = \frac{2}{3} \begin{pmatrix} 2 & -1/2 & \cdots & 0 & 0 \\ 0 & 0 & \cdots & \cdots & 0 \\ \vdots & & & \vdots & \\ 0 & 0 & \cdots & -1/2 & 2 \end{pmatrix} \in \mathbb{R}^{n \times n}$$

contains the Neumann boundary conditions (see e.g., [12]), then the coefficient matrices of 6 are defined as

$$\mathbf{A}_{11} = \Gamma \mathbf{I}_n + \frac{\delta_1}{\ell_x^2} \mathbf{T}, \quad \mathbf{A}_{21} = -\Gamma\beta h \mathbf{I}_n + \frac{\delta_2}{\ell_x^2} \mathbf{T}, \quad \mathbf{A}_{12} = \frac{\delta_1}{\ell_y^2} \mathbf{T}, \quad \text{and} \quad \mathbf{A}_{22} = \frac{\delta_2}{\ell_y^2} \mathbf{T}$$

where $\ell_x = \ell_y = 2/(n - 1)$. Notice that the discretized linear terms $\Gamma \mathbf{U}_1$ and $-\Gamma\beta h \mathbf{U}_2$ have been incorporated into the coefficient matrices \mathbf{A}_{11} and \mathbf{A}_{21} respectively. Furthermore the matrix $\mathcal{F}_1(\mathbf{U}_1, \mathbf{U}_2, t)$ stems from evaluating the function $f_1(u_1, u_2) = -\Gamma u_1^3$ elementwise, whereas $\mathcal{F}_2(\mathbf{U}_1, \mathbf{U}_2, t) = \Gamma\beta \mathbf{U}_1$ is linear and requires no HO-DEIM interpolation. Finally, the remaining linear term in the first equation $-\Gamma \mathbf{U}_2$ can be projected explicitly onto the HO-POD subspace of the first equation.

In our experiments we found that $n_s = 20$ equispaced snapshots $\mathbf{U}_1(t)$ and $\mathbf{U}_2(t)$ in the timespan $[0, 1]$ are sufficient for constructing the basis vectors. Furthermore, we consider four different truncation tolerances ($\tau = 10^{-2}, 10^{-4}, 10^{-6}, 10^{-8}$) for this experiment. Table 1 reports all the basis dimensions obtained for each τ , by means of 29.

TABLE 1. Example 1. Dim. of HO-POD and HO-DEIM bases obtained for different τ . The full order model has dimension $n = 1200$.

τ	\mathbf{U}_i	left dim. HO-POD	right dim. HO-POD	left dim. HO-DEIM	right dim. HO-DEIM
10^{-2}	$\bar{\mathbf{U}}_1$	7	7	11	11
	$\bar{\mathbf{U}}_2$	9	10	–	–
10^{-4}	$\bar{\mathbf{U}}_1$	18	20	23	23
	$\bar{\mathbf{U}}_2$	19	20	–	–
10^{-6}	$\bar{\mathbf{U}}_1$	31	33	32	34
	$\bar{\mathbf{U}}_2$	29	31	–	–
10^{-8}	$\bar{\mathbf{U}}_1$	43	46	44	47
	$\bar{\mathbf{U}}_2$	37	40	–	–

In Figure 1 (left) we plot the average error 28 for both $\tilde{\mathbf{U}}_1$ and $\tilde{\mathbf{U}}_2$ integrated from 0 to t_f at $n_t = 300$ timesteps, for the different values of τ presented in Table 1.

For the error computation, both the full order model and the reduced order model are integrated with the IMEX 2-SBDF scheme. On the right of Figure 1 we plot the CPU time for integrating the full order model and the reduced order model at $n_t = 300$ timesteps for decreasing τ . The figures indicate that even when the

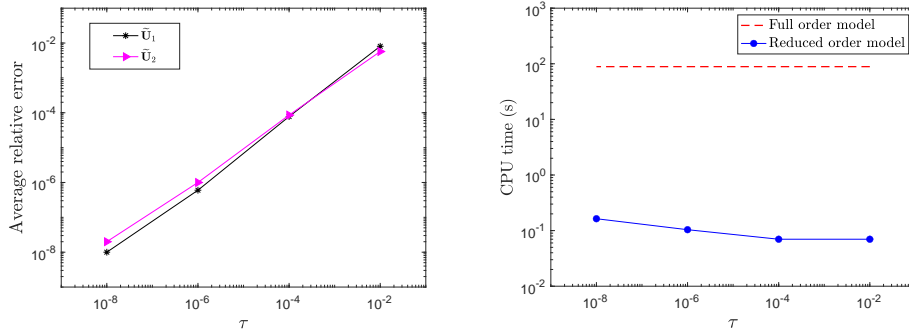


FIGURE 1. Example 1: Average relative error 28 (left) and online computational time (right) of the reduced order model and the full order model for different values of τ .

HO-POD-DEIM reduced order model approximates the full order model with eight digits of accuracy, the time needed to integrate the model is almost three orders of magnitude faster. \square

In what follows we analyze the efficiency of the offline phase and compare the procedure to the standard POD-DEIM procedure applied to the 2D Burgers equation in [53].

Example 2. *The 2D coupled Burgers equation (BE)* [53]. Here we consider the semilinear 2D coupled Burgers equation given by

$$\begin{cases} \dot{u}_1 = \frac{1}{r} \Delta u_1 - u_1(u_1)_x - u_2(u_1)_y \\ \dot{u}_2 = \frac{1}{r} \Delta u_2 - u_1(u_2)_x - u_2(u_2)_y \end{cases} \quad (31)$$

where $u_1(x, y, t)$ and $u_2(x, y, t)$ ($t \in [0, 1]$) are the velocities to be determined, with $(x, y) \in [0, 1]^2$, and r is the Reynold's number. As is done in [53], we derive the initial and boundary conditions from the exact traveling wave solution of the 2D Burgers equation, given by (see e.g., [15])

$$u_1(x, y, t) = \frac{3}{4} - \frac{1}{4} \left(1 + e^{\frac{r(-4x+4y-t)}{32}} \right)^{-1} \quad u_2(x, y, t) = \frac{3}{4} + \frac{1}{4} \left(1 + e^{\frac{r(-4x+4y-t)}{32}} \right)^{-1}.$$

We consider the case $r = 100$ and discretize the model on a grid with n spatial nodes in each direction, yielding a system of the form 6, with nonlinear functions

$$\mathcal{F}_i(\mathcal{D}_i(\mathbf{u}_i), \mathbf{u}_1, \mathbf{u}_2, t) = \mathcal{F}_i(\mathcal{D}_i(\mathbf{U}_i), \mathbf{U}_1, \mathbf{U}_2, t) := (\mathbf{B}_{1i} \mathbf{U}_i) \circ \mathbf{U}_1 + (\mathbf{U}_i \mathbf{B}_{2i}^\top) \circ \mathbf{U}_2, \quad (32)$$

for $i = 1, 2$, where the matrices $\mathbf{B}_{1i} \in \mathbb{R}^{n \times n}$ and $\mathbf{B}_{2i} \in \mathbb{R}^{n \times n}$ contain the coefficients for a first order centered difference space discretization in the x - and y - directions respectively (i.e., $\mathbf{B}_{1i} = \mathbf{B}_{2i} = \frac{n-1}{2} \text{tridiag}(-1, \mathbf{0}, 1)$), and \circ is the matrix Hadamard product. An upwind scheme can also be considered for \mathbf{B}_{1i} and \mathbf{B}_{2i} , as is typically done for the coupled Burgers equation, however, in order to reproduce the results of [53] we consider centered finite differences.

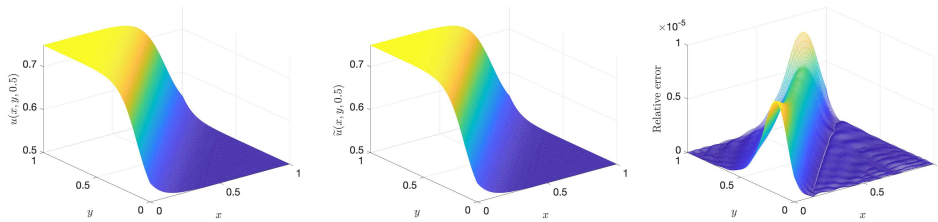


FIGURE 2. Example 2: $u_1(x, y, 0.5)$ discretized with $n = 200$. The exact solution (left), the HO-POD-DEIM approximation (middle), and the relative error mesh between the two (right).

It is also worth motivating the use of DEIM for the nonlinear function 32. Indeed, this type of nonlinearity can also be efficiently treated in the vectorized POD reduced model by writing it as a tensor (see e.g., [32]) in order to avoid the use of DEIM. Nevertheless, in [48, Table I] this idea is compared to that of POD-DEIM and it is concluded that for quadratic nonlinearities the POD-DEIM model requires considerably fewer floating point operations online for moderate DEIM dimension p . Furthermore, we use DEIM to reproduce and compare to the results of [53], where it is indeed used.

As mentioned above, the presented HO-POD-DEIM order reduction strategy is compared to the standard POD-DEIM applied to 31 in [53]. We did not have access to the codes of [53], but the POD-DEIM algorithm was implemented as discussed in their paper and the results in terms of basis dimension to accuracy are comparable to the ones reported in [53]. Moreover, in [53], the reduced order model is integrated by a fully implicit scheme, whereas for this experiment we use the IMEX 2-SBDF method to integrate both the HO-POD-DEIM and POD-DEIM reduced order models, which accounts for the faster online phase for POD-DEIM in comparison to the times reported in [53].

To this end, we consider four different space discretizations ($n = 60, 200, 600, 1200$) and compare the computational details of HO-POD-DEIM to that of POD-DEIM [53]. Therefore, to ensure stability in the numerical integration we consider $n_t = 2n$ discrete timesteps for integrating the reduced order model. Moreover, to correspond with the space discretization error, we set $\tau = 1/n^2$.

In our experiments, we have observed that the HO-POD-DEIM strategy requires far fewer snapshots than POD-DEIM to construct an equally accurate reduced order model. We hypothesize that this is because one matrix snapshot contains information about several spatial directions in \mathbb{R}^n , whereas one vector snapshot only offers information about one spatial direction in \mathbb{R}^N . Therefore, to obtain a POD basis of dimension k in the vectorized setting, at least k snapshots are required, even though one vector in \mathbb{R}^N contains many spatial directions from \mathbb{R}^n . A further experimental or theoretical analysis of the relationship between array snapshots and vectorized snapshots could be interesting in future work. To this end, we consider $n_s = 20$ equispaced snapshots for HO-POD-DEIM and $n_s = 100$ for POD-DEIM.

A visual comparison of the accuracy of the HO-POD-DEIM reduced model at $t = 0.5$, when $n = 200$ is plotted in Figures 2 and 3 for u_1 and u_2 respectively. Moreover, in Figure 4 we plot the average relative error through $n_t = 2n$ timesteps between the HO-POD-DEIM approximation and the exact solution at the relevant nodes, for the

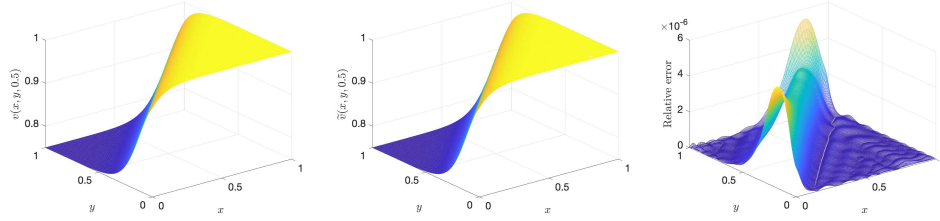


FIGURE 3. Example 2: $u_2(x, y, 0.5)$ discretized with $n = 200$. The exact solution (left), the HO-POD-DEIM approximation (middle), and the relative error mesh between the two (right).

four different space dimensions n . We investigate the computational load required by both strategies to achieve this accuracy.

Firstly, we report in Table 2 the reduced basis dimensions for HO-POD-DEIM and POD-DEIM for all four space discretizations, as well as the memory requirements. In particular, for each \mathbf{U}_i we report the dimensions k_1/k_2 (p_1/p_2) of the HO-POD (HO-DEIM) bases and the dimension k (p) of the POD (DEIM) bases. Moreover, the reported global memory requirements include the number of stored vectors multiplied by their length ($\# \cdot length$) in each phase. The table indicates a great

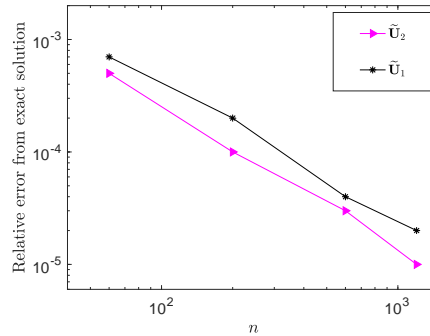


FIGURE 4. Example 2: The average relative error through $n_t = 2n$ timesteps between the HO-POD-DEIM approximation $\tilde{\mathbf{U}}_1(t)$ ($\tilde{\mathbf{U}}_2(t)$) and the exact solution $u_1(x, y, t)$ ($u_2(x, y, t)$).

reduction in memory requirements for HO-POD-DEIM in comparison to POD-DEIM, but the POD-DEIM strategy produces a smaller reduced order model, as is expected from a one-sided reduction strategy. That is, the POD-DEIM reduced model requires evaluating the nonlinear function at merely p entries, whereas the HO-POD-DEIM reduced model requires evaluating the nonlinear function at $p_1 \cdot p_2$ entries. From Table 2 it is clear that $p_1 \cdot p_2 \geq p$ for all n .

We investigate the pros and cons, in terms of computational time, of both strategies in Figure 5. On the left of Figure 5 we plot the time needed offline to construct the basis vectors for both strategies, for increasing n . For HO-POD-DEIM this includes the time needed to perform the SVD of each snapshot and the time needed

TABLE 2. A breakdown of the (HO)-POD and (HO)-DEIM basis dimensions and the memory requirements for four different state space dimensions. Note that $\tau = 1/n^2$.

n	ALGORITHM	\mathbf{U}_i	POD DIM.	DEIM DIM.	OFFLINE MEMORY	ONLINE MEMORY
60	HO-POD-DEIM	\mathbf{U}_1	9/9	18/18	$98n$	$54n$
		\mathbf{U}_2	9/9	18/18	$98n$	$54n$
	POD-DEIM [53]	\mathbf{U}_1	5	14	$400n^2$	$19n^2$
		\mathbf{U}_2	4	14	$400n^2$	$18n^2$
200	HO-POD-DEIM	\mathbf{U}_1	13/13	24/25	$153n$	$75n$
		\mathbf{U}_2	12/12	24/25	$153n$	$73n$
	POD-DEIM [53]	\mathbf{U}_1	9	23	$400n^2$	$32n^2$
		\mathbf{U}_2	8	23	$400n^2$	$31n^2$
600	HO-POD-DEIM	\mathbf{U}_1	16/17	32/32	$196n$	$97n$
		\mathbf{U}_2	16/16	32/32	$194n$	$96n$
	POD-DEIM [53]	\mathbf{U}_1	15	28	$400n^2$	$43n^2$
		\mathbf{U}_2	14	28	$400n^2$	$42n^2$
1200	HO-POD-DEIM	\mathbf{U}_1	19/19	36/39	$219n$	$113n$
		\mathbf{U}_2	19/19	36/39	$215n$	$113n$
	POD-DEIM [53]	\mathbf{U}_1	19	31	$400n^2$	$50n^2$
		\mathbf{U}_2	18	31	$400n^2$	$50n^2$

to orthogonalize and truncate the new basis vectors for all 8 bases⁵, whereas for POD-DEIM this includes the time to vectorize each snapshot and the time to perform the economy SVD of all four $n^2 \times n_s$ matrices of snapshots. On the right of Figure 5 we report the time needed to evaluate 22 and a system of the form 8 at n_t timesteps online and compare it to the time needed to evaluate the full order model 6. The timings in Figure 5 (right) correspond to the reduced dimensions reported in Table 2.

Figure 5 (left) indicates the large gain in offline computational time by the new strategy, with almost two orders of magnitude difference as n increases. However, due to the larger reduced dimensions of HO-POD-DEIM reported in Table 2, fractionally more time is required online, as presented in Figure 5 (right). Nevertheless the online times are very comparable and orders of magnitude lower than the full order model 6. In problems where the nonlinear term is more expensive to evaluate this drawback of HO-POD-DEIM will become more evident, however, and will need to be further investigated in future work; see also Remark 1.

This experiment indicated that a greater accuracy with respect to the exact solution can be achieved by the discrete HO-POD-DEIM reduced order model in a fraction of the offline computational time compared to POD-DEIM. Moreover the online time remains comparable, and a large gain in memory requirements is witnessed. \square

In what follows we illustrate the efficiency of the procedure in the multilinear setting.

⁵Each equation u_1 and u_2 require four basis matrices when $d = 2$. Two stemming from the snapshot solutions $\{\mathbf{U}_i(t_j)\}_{j=1}^{n_s}$ for the HO-POD dimension reduction and two stemming from the nonlinear snapshots 27 for the HO-DEIM interpolation.

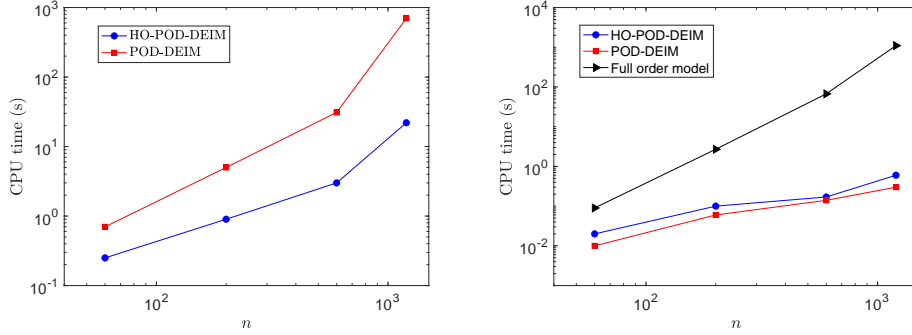


FIGURE 5. Example 2: A comparison of the time required offline for basis construction (left) and online for integration (right) between HO-POD-DEIM and POD-DEIM [53] for increasing n .

Example 3. *The 3D coupled Burgers equation (BE).* Here we consider the semi-linear 3D coupled Burgers equation (see, e.g., [17]) given by

$$\begin{cases} \dot{u}_1 &= \frac{1}{r}\Delta u_1 - \underline{u} \cdot \nabla u_1 \\ \dot{u}_2 &= \frac{1}{r}\Delta u_2 - \underline{u} \cdot \nabla u_2, \\ \dot{u}_3 &= \frac{1}{r}\Delta u_3 - \underline{u} \cdot \nabla u_3, \end{cases} \quad (33)$$

where $u_1(x, y, z, t)$, $u_2(x, y, z, t)$ and $u_3(x, y, z, t)$ are the three velocities to be determined, with $(x, y, z) \in [0, 1]^3$ and $t \in [0, 1]$. Furthermore, the system is subject to homogeneous Dirichlet boundary conditions and initial states

$$\begin{aligned} u_1(x, y, z, 0) &= \frac{1}{10} \sin(2\pi x) \sin(2\pi y) \cos(2\pi z) \\ u_2(x, y, z, 0) &= \frac{1}{10} \sin(2\pi x) \cos(2\pi y) \sin(2\pi z) \\ u_3(x, y, z, 0) &= \frac{1}{10} \cos(2\pi x) \sin(2\pi y) \sin(2\pi z). \end{aligned}$$

A finite difference space discretization inside the cube yields a system of ODEs of the form 6, with nonlinear functions given by

$$\mathcal{F}_i(\mathcal{D}_i(\mathbf{u}_i), \mathbf{u}_1, \mathbf{u}_2, \mathbf{u}_3, t) = (\mathbf{u}_i \times_1 \mathbf{B}_{1i}) \circ \mathbf{u}_1 + (\mathbf{u}_i \times_2 \mathbf{B}_{2i}) \circ \mathbf{u}_2 + (\mathbf{u}_i \times_3 \mathbf{B}_{3i}) \circ \mathbf{u}_3,$$

for $i = 1, 2, 3$, where $\mathbf{B}_{1i} \in \mathbb{R}^{n \times n}$, $\mathbf{B}_{2i} \in \mathbb{R}^{n \times n}$ and $\mathbf{B}_{3i} \in \mathbb{R}^{n \times n}$ contain the coefficients for a first order centered difference space discretization in the x -, y - and z - directions respectively. Furthermore we vary r through the experiment, and calculate the reduced order model through $n_s = 50$ equispaced snapshots for both HO-POD-DEIM and POD-DEIM.

Firstly, we set $r = 10$ and consider five different space discretizations ($n = 50, 80, 100, 150, 200$) and investigate the efficiency of the offline phase of the HO-POD-DEIM procedure for systems when $d = 3$, in comparison to standard POD-DEIM. Note that the system 6 of dimension $n = 200$ is equivalent to the system 2 with dimension $N = 8\,000\,000$ when $d = 3$.

The improvement in memory requirements is immediately evident, since the new procedure requires storing basis vectors of length n , whereas the vectorization procedure needs to store many basis vectors of length n^3 , as has been witnessed in

Table 2 for $d = 2$. In Figure 6 (left) we compare the computational time needed to

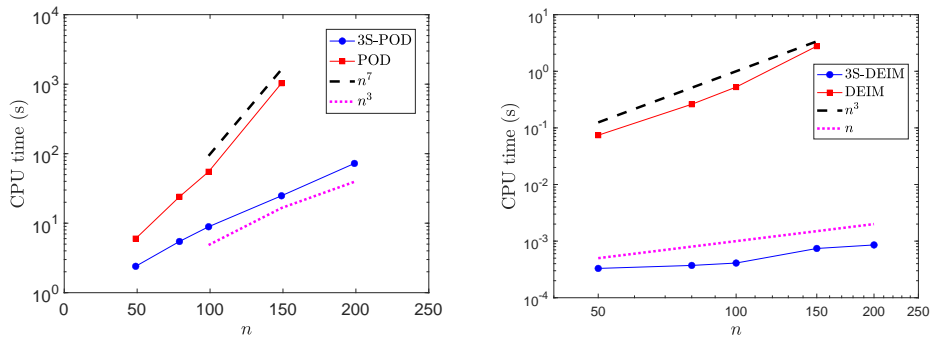


FIGURE 6. Example 3: A comparison of the offline time for increasing dimension n , between HO-POD and POD (left) and HO-DEIM and DEIM (right).

determine the basis vectors, given $\tau = 10^{-4}$, for increasing dimension n . For the new procedure that includes the time needed to perform the STHOSVD of each snapshot and the time needed to orthogonalize and truncate the new basis vectors, whereas for POD-DEIM this includes the time to vectorize each snapshot and the time to perform the economy SVD of the $n^3 \times n_s$ matrix of snapshots. The times are added together for all 18 bases⁶ required by HO-POD-DEIM and all 6 bases required by POD-DEIM. We explicitly remark that both the STHOSVD and the economy SVD can potentially be further accelerated by using randomized algorithms; see e.g., [21, 36]. This is, however, not considered in our experiments.

In Figure 6 (right) we compare the time needed to determine the (HO)-DEIM interpolation indices. That is, the cumulative time taken by `q-deim` for all 9 nonlinear bases for HO-POD-DEIM and all 3 nonlinear bases required by POD-DEIM.

For both POD and DEIM the improvement in computational time is very evident in the plots, with a few orders of magnitude difference. On the standard laptop computer on which these experiments were performed, the HO-POD-DEIM bases were created in just more than a minute for $n = 200$, whereas for the vectorization procedure, the computer ran out of memory, after processing 30 snapshots in more than an hour.

In what follows we investigate the online phase. We set $n = 150$ and illustrate the efficiency of the three-sided reduction procedure, together with the new T3-SYLV method for solving the low-dimensional, dense tensor-valued system of equations. To this end we investigate the total time needed for solving all inner linear systems at $n_t = 100$ timesteps, that is 300 linear systems in total, using T3-SYLV and compare it to the time needed if the system 25 is vectorized and solved as a standard (nearly dense) linear system (Vec-lin). This is done for different values of τ , which result in different reduced dimensions. In particular, we plot the computational time with

⁶Each equation u_1, u_2 and u_3 requires six basis matrices when $d = 3$. Three stemming from the snapshot solutions $\{\mathbf{u}_i(t_j)\}_{j=1}^{n_s}$ for the HO-POD dimension reduction and three stemming from the nonlinear snapshots 27 for the HO-DEIM interpolation. For standard POD-DEIM each equation requires only two basis matrices, one for dimension reduction and one for DEIM interpolation, hence six bases in total.

respect to the maximum dimension of the vectorized systems for the different values of τ . That is, the value $\max(k_1 k_2 k_3)$ on the x -axis is the maximum value of $k_{1i} k_{2i} k_{3i}$ for all $i = 1, 2, 3$, given τ .

For the solution of the vectorized system we perform a reverse Cuthill–McKee reordering of the coefficient matrices, to exploit any remaining sparsity pattern, and perform an LU decomposition once for all, so that only front- and back-substitution is required for all system solves. The results are reported in Figure 7.

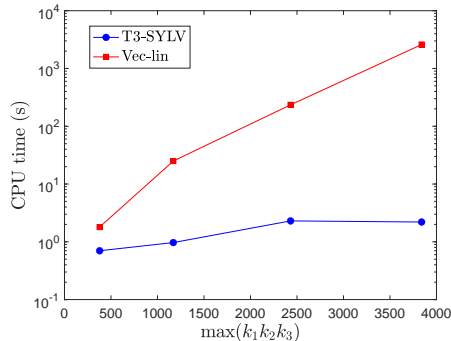


FIGURE 7. Example 3: A comparison of the time to solve all linear systems of the form 25, for different values of τ , between T3-SYLV and Vec-lin. The x -axis displays the maximum dimension of the three vectorized equations for different values of τ .

The advantage that the three-sided reduction procedure poses in combination with the T3-SYLV inner solver is evident from Figure 7. This figure, together with Figure 6 illustrates that a lot of time can be saved offline and online. Without the T3-SYLV inner solver it is evident that the tensor structure of the coefficient matrices retained by the three sided projection would result in expensive, dense linear system solves, which would cancel the time that has been saved in the offline phase. Nevertheless, with the availability of the T3-SYLV solver, a large speedup is seen in both the offline and online phases, together with a massive gain in memory requirements.

Finally, Table 3 and Table 4 contain the details of the reduced order model, given $n = 150$, $\tau = 10^{-4}$ and the error measure 28 for increasing values of the Reynold’s number r . Table 3 illustrates that a large reduction in all dimensions is achieved, with a very acceptable accuracy over 300 timesteps, even for large r . Nevertheless it is clear that for larger Reynold’s number the singular value decay in each mode becomes slower, resulting in larger reduced dimensions. Moreover we mention that for this same problem, when $r = 100$, standard POD-DEIM would require storing 57 vectors of length n^3 in the online phase, as opposed to the 245 vectors of length n that need to be stored for HO-POD-DEIM. Furthermore, Table 4 confirms that even for large r we observe a large gain in online computational time achieved by the reduced model. \square

Example 4. *A 3D reaction-diffusion model for cell apoptosis.* As a final example we consider a reaction-diffusion system, originally introduced in [10] to investigate the behavior of protein concentrations (in space and time) of a cell apoptosis model

TABLE 3. Example 3. Dim. of HO-POD and HO-DEIM bases and the average error at 300 timesteps for increasing r . The full order model has dimension $n = 150$ and $\tau = 10^{-4}$.

r	u	k_1	k_2	k_3	p_1	p_2	p_3	ERROR $\bar{\mathcal{E}}(\mathbf{U})$
10	u_1	4	7	10	7	12	16	$1 \cdot 10^{-4}$
	u_2	7	7	7	9	12	13	$6 \cdot 10^{-5}$
	u_3	8	12	8	9	16	13	$1 \cdot 10^{-4}$
100	u_1	6	11	15	10	17	20	$3 \cdot 10^{-5}$
	u_2	10	11	11	12	17	17	$4 \cdot 10^{-5}$
	u_3	10	16	12	12	21	17	$4 \cdot 10^{-5}$
500	u_1	9	15	19	13	23	26	$2 \cdot 10^{-5}$
	u_2	11	16	17	14	23	23	$3 \cdot 10^{-5}$
	u_3	12	19	16	14	25	23	$4 \cdot 10^{-5}$

 TABLE 4. Example 3. Memory and CPU time required for basis construction and integration. The full order model has dimension $n = 150$ and $\tau = 10^{-4}$.

r	Online memory	Basis time(s)	FOM time(s)	ROM time(s)
10	$177n$	20	1641	1.9
100	$245n$	20	1641	2.2
500	$318n$	20	1641	3.3

in 1D. The model was later extended to higher dimension in [11, Chapter 2.3]. The proteins build a network called ‘‘caspase–cascade’’ and the dynamics, with homogeneous Neumann boundary conditions, are given by

$$\begin{aligned}
 \dot{u}_1 &= \delta_1 \Delta u_1 - c_4 u_1 + c_1 \sin(u_3 u_2), & \dot{u}_2 &= \delta_2 \Delta u_2 - c_4 u_2 + c_2 u_4 u_1^3, \\
 \dot{u}_3 &= \delta_3 \Delta u_3 - c_4 u_3 - c_1 \sin(u_3 u_2) + c_3, & \dot{u}_4 &= \delta_4 \Delta u_4 - c_4 u_4 - c_2 u_4 u_1^3 + c_3,
 \end{aligned} \tag{34}$$

where $u_1(\mathbf{x}, t)$, $u_2(\mathbf{x}, t)$, $u_3(\mathbf{x}, t)$ and $u_4(\mathbf{x}, t)$ are four different reactants called Procaspase-8, Procaspase-3, Caspase-8 and Caspase-3 respectively, with $\mathbf{x} = (x, y, z) \in [0, 1]^3 =: \Omega$ and $t \in [0, 1]$. For the values and derivation of the constants δ_i and c_i we refer the reader to [11, Chapter 2.3] and we consider the initial condition

$$(u_1, u_2, u_3, u_4)(\mathbf{x}, 0) = \begin{cases} \left(u_1^{(d)}, u_2^{(d)}, u_3^{(d)}, u_4^{(d)} \right) & \text{for } \mathbf{x} \in \Omega_{\text{ext}} \\ \left(u_1^{(\ell)}, u_2^{(\ell)}, u_3^{(\ell)}, u_4^{(\ell)} \right) & \text{for } \mathbf{x} \in \Omega_{\text{in}} \end{cases},$$

where $\Omega_{\text{ext}} := \{\mathbf{x} \in \Omega, r_0 \leq \|\mathbf{x}\|_2 \leq 1\}$ and $\Omega_{\text{in}} := \{\mathbf{x} \in \Omega, \|\mathbf{x}\|_2 < r_0\}$ and we consider $r_0 = \{0.1, 0.3\}$. Furthermore, $u_i^{(\ell)}$ and $u_i^{(d)}$ represent respectively the life and death states of the reactants and they are defined in [11, Chapter 2.4]. Note that we have introduced the sin function in equations one and three to also test the strength of the procedure on non-polynomial nonlinearities.

For the experimental setup we discretize 34 with $n = 150$ nodes in each of the spatial directions. Therefore, if $\mathbf{T} \in \mathbb{R}^{n \times n}$ is defined as in Example 1, this yields a

system of the form 6, with

$$\mathbf{A}_{1i} = -c_4 \mathbf{I}_n - \frac{\delta_i}{\ell_x^2} \mathbf{T}, \quad \mathbf{A}_{2i} = \frac{\delta_i}{\ell_y^2} \mathbf{T}, \quad \mathbf{A}_{3i} = \frac{\delta_i}{\ell_z^2} \mathbf{T}, \quad i = 1, 2, 3, 4,$$

and $\ell_x = \ell_y = \ell_z = 1/(n-1)$, where the additional linear terms have been incorporated into the matrices \mathbf{A}_{1i} . Furthermore, the nonlinear functions $\mathcal{F}_1(\mathbf{u}_1, \mathbf{u}_2, \mathbf{u}_3, \mathbf{u}_4, t)$ and $\mathcal{F}_2(\mathbf{u}_1, \mathbf{u}_2, \mathbf{u}_3, \mathbf{u}_4, t)$ stem from respectively evaluating the nonlinear terms $c_1 \sin(u_3 u_2)$ and $c_2 u_4 u_1^3$ elementwise. Notice, furthermore, that $\mathcal{F}_3 = -\mathcal{F}_1$ and $\mathcal{F}_4 = -\mathcal{F}_2$, so that only two HO-DEIM bases are required, instead of four. The constant matrices stemming from the discretization of the constant c_3 are treated separately. Finally we consider $\tau = 10^{-2}$ and $n_s = 30$ equispaced snapshots of each \mathbf{u}_i , \mathcal{F}_1 and \mathcal{F}_2 in the timespan.

In Table 5 we report, for all four equations and both values of r_0 , the dimension of the HO-POD and HO-DEIM bases, the online memory requirements (# of vectors times the length, as before), the online time for $n_t = 300$ (for each equation separately) and the average relative error 28.

TABLE 5. Example 4. Dim. of HO-POD and HO-DEIM bases and further computational details for $\tau = 10^{-2}$ and $n = 150$.

r_0	\mathbf{U}_i	POD DIM. ($k_1/k_2/k_3$)	DEIM DIM. ($p_1/p_2/p_3$)	ONLINE MEMORY	ONLINE TIME (S)	ERROR
0.1	\mathbf{U}_1	2/2/2	5/5/5	$21n$	1.29	$3 \cdot 10^{-4}$
	\mathbf{U}_2	2/2/2	3/3/3	$15n$	1.20	$4 \cdot 10^{-4}$
	\mathbf{U}_3	18/18/18	–	$54n$	1.50	$3 \cdot 10^{-4}$
	\mathbf{U}_4	9/9/9	–	$27n$	0.63	$1 \cdot 10^{-2}$
0.3	\mathbf{U}_1	8/8/8	9/9/9	$51n$	1.56	$3 \cdot 10^{-4}$
	\mathbf{U}_2	8/8/8	9/9/9	$51n$	1.13	$3 \cdot 10^{-4}$
	\mathbf{U}_3	43/43/42	–	$128n$	11.25	$3 \cdot 10^{-3}$
	\mathbf{U}_4	31/31/30	–	$92n$	4.27	$5 \cdot 10^{-3}$

We observe a large decrease in the state dimension for both values of r_0 , with a very acceptable average relative error in all equations. Equations three and four require a larger basis than one and two, but in turn they do not require the additional cost online of HO-DEIM interpolation and the evaluation of the nonlinear function. Furthermore, we observe that all equations can be solved in a rapid online phase, whereas the full order model needs approximately 4064 seconds to be integrated at $n_t = 300$ timesteps, independent of r_0 . \square

7. Conclusion. In this paper we have illustrated that systems of the form 1, with linear operators with separable coefficients, discretized by a tensor basis on certain domains, can be treated directly in array form. In this setting, we have extended the POD-DEIM model order reduction method to the multilinear setting and illustrated how it can be used to massively reduce the dimension and complexity of systems of ODEs in two and three spatial dimensions. Some very encouraging numerical experiments on difficult problems such as the 2D and 3D viscous Burgers equation, indicate a dramatic decrease in both CPU time and memory requirements in the offline phase for constructing the bases, especially when $d = 3$.

Nevertheless, the dense Kronecker structure of the reduced order model obtained by the HO-POD-DEIM projection would incur unnecessary computational costs in the online phase when $d = 3$. To this end we have shown how the novel T3-SYLV linear system solver from [46] can exploit the structure of the reduced order model, resulting in a large decrease in computational time in the online phase as well.

Future work would entail an analysis of the number of snapshots required by HO-POD-DEIM in comparison to POD-DEIM. It could also be of interest to extend the T3-SYLV solver to higher dimensions so that the HO-POD-DEIM strategy can be applied to PDEs with $d > 3$. Furthermore, the extension to the parameter dependent setting can also be considered. This will result in an additional dimension that needs to be treated. Finally, the presented algorithm can certainly also benefit from a dynamic implementation as presented in the companion manuscript [28].

Acknowledgments. We thank Valeria Simoncini for her support and careful reading of earlier versions of this manuscript. We are also grateful to the two anonymous referees for their careful reading and helpful suggestions, which helped improve the presentation.

REFERENCES

- [1] A. Antoulas, C. Beattie and S. Gugercin, *Interpolatory methods for model reduction*, SIAM, Philadelphia, 2020.
- [2] U. M. Ascher, S. J. Ruuth and B. T. Wetton, Implicit-explicit methods for time-dependent partial differential equations, *SIAM J. Numer. Anal.*, **32** (1995), 797–823.
- [3] P. Astrid, S. Weiland, K. Willcox and T. Backx, Missing point estimation in models described by proper orthogonal decomposition, *IEEE Trans. Autom. Control*, **53** (2008), 2237–2251.
- [4] M. Barrault, Y. Maday, N. C. Nguyen and A. T. Patera, An ‘empirical interpolation’ method: application to efficient reduced-basis discretization of partial differential equations, *C. R. Math. Acad. Sci. Paris*, **339** (2004), 667–672.
- [5] P. Benner, V. Mehrmann and D. Sorensen, *Dimension reduction of large-scale systems*, Springer-Verlag, Berlin/Heidelberg, Germany, 2005.
- [6] P. Benner, S. Gugercin and K. Willcox, A survey of projection-based model reduction methods for parametric dynamical systems, *SIAM Rev.*, **57** (2015), 483–531.
- [7] D. Bonomi, A. Manzoni and A. Quarteroni, A matrix DEIM technique for model reduction of nonlinear parametrized problems in cardiac mechanics, *Comput. Methods Appl. Mech. Eng.*, **324** (2017), 300–326.
- [8] S. Chaturantabut and D. C. Sorensen, Nonlinear model reduction via discrete empirical interpolation, *SIAM J. Sci. Comput.*, **32** (2010), 2737–2764.
- [9] S. Chaturantabut and D. C. Sorensen, Application of POD and DEIM on dimension reduction of non-linear miscible viscous fingering in porous media, *Math. Comput. Modell. Dyn. Syst.*, **17** (2011), 337–353.
- [10] M. Daub, S. Waldherr, F. Allgöwer, P. Scheurich and G. Schneider, Death wins against life in a spatially extended apoptosis model, *Biosystems*, **108** (2012), 45–51.
- [11] M. Daub, *Mathematical modeling and numerical simulations of the extrinsic pro-apoptotic signaling pathway*, PhD thesis, University of Stuttgart, 2013.
- [12] M. C. D’Autilia, I. Sgura and V. Simoncini, Matrix-oriented discretization methods for reaction–diffusion PDEs: Comparisons and applications, *Computers & Mathematics with Applications*, 2067–2085.
- [13] A. De Wit, *Spatial Patterns and Spatiotemporal Dynamics in Chemical Systems*, 435–513, John Wiley & Sons, Ltd, 1999, URL <https://onlinelibrary.wiley.com/doi/abs/10.1002/9780470141687.ch5>.
- [14] Z. Drmač and S. Gugercin, A new selection operator for the discrete empirical interpolation method—improved a priori error bound and extensions, *SIAM J. Sci. Comput.*, **38** (2016), A631–A648.
- [15] C. A. Fletcher, Generating exact solutions of the two-dimensional Burgers’ equations, *Int. J. Numer. Methods Fluids*, **3** (1983), 213–216.

- [16] G. Gambino, M. Lombardo and M. Sammartino, Pattern selection in the 2D FitzHugh–Nagumo model, *Ricerche di Matematica*, **68** (2019), 535–549.
- [17] Q. Gao and M. Zou, An analytical solution for two and three dimensional nonlinear Burgers’ equation, *Appl. Math. Modell.*, **45** (2017), 255 – 270, URL <http://www.sciencedirect.com/science/article/pii/S0307904X16306710>.
- [18] U. Z. George, A. Stéphanou and A. Madzvamuse, Mathematical modelling and numerical simulations of actin dynamics in the eukaryotic cell, *J Math Biol*, **66** (2013), 547–593.
- [19] G. H. Golub and C. F. van Loan, *Matrix Computations*, 4th edition, Johns Hopkins University Press, Baltimore, 2013, URL <http://www.cs.cornell.edu/cv/GVL4/golubandvanloan.htm>.
- [20] C. Gu, QLMOR: A projection-based nonlinear model order reduction approach using quadratic-linear representation of nonlinear systems, *IEEE Trans. Comput.-Aided Design Integr. Circuits Syst.*, **30** (2011), 1307–1320.
- [21] N. Halko, P.-G. Martinsson and J. A. Tropp, Finding structure with randomness: Probabilistic algorithms for constructing approximate matrix decompositions, *SIAM Rev*, **53** (2011), 217–288.
- [22] M. Hinze and S. Volkwein, Proper orthogonal decomposition surrogate models for nonlinear dynamical systems: Error estimates and suboptimal control, in *Dimension reduction of large-scale systems*, Springer, 2005, 261–306.
- [23] A. L. Hodgkin and A. F. Huxley, A quantitative description of membrane current and its application to conduction and excitation in nerve, *The Journal of physiology*, **117** (1952), 500–544.
- [24] W. Hundsdorfer and J. G. Verwer, *Numerical solution of time-dependent advection-diffusion-reaction equations*, vol. 33, Springer Science & Business Media, 2013.
- [25] B. Karasözen, M. Uzunca and T. Küçükseyhan, Model order reduction for pattern formation in Fitzhugh–Nagumo equations, in *Numerical Mathematics and Advanced Applications ENUMATH 2015*, Springer, 2016, 369–377.
- [26] B. Karasözen, M. Uzunca and T. Küçükseyhan, Reduced order optimal control of the convective Fitzhugh–Nagumo equations, *Computers & Mathematics with Applications*, **79** (2020), 982–995.
- [27] B. Karasözen, S. Yıldız and M. Uzunca, Structure preserving model order reduction of shallow water equations, *Mathematical Methods in the Applied Sciences*, **44** (2021), 476–492.
- [28] G. Kirsten and V. Simoncini, A matrix-oriented POD-DEIM algorithm applied to nonlinear differential matrix equations, *arXiv preprint arXiv:2006.13289*.
- [29] T. G. Kolda and B. W. Bader, Tensor decompositions and applications, *SIAM Rev*, **51** (2009), 455–500.
- [30] B. Kramer, *Model reduction of the coupled Burgers equation in conservation form*, PhD thesis, Virginia Tech, 2011.
- [31] B. Kramer and K. E. Willcox, Nonlinear model order reduction via lifting transformations and proper orthogonal decomposition, *AIAA Journal*, **57** (2019), 2297–2307.
- [32] K. Kunisch and S. Volkwein, Control of the Burgers equation by a reduced-order approach using proper orthogonal decomposition, *J. Optim. theory Appl.*, **102** (1999), 345–371.
- [33] P. K. Maini and H. G. Othmer, *Mathematical Models for Biological Pattern Formation*, The IMA Volumes in Mathematics and its Applications - Frontiers in application of Mathematics, Springer-Verlag, New York, 2001.
- [34] H. Malchow, S. Petrovskii and E. Venturino, *Spatiotemporal Patterns in Ecology and Epidemiology: Theory, Models, and Simulations*, Chapman & Hall, CRC, London, 2008.
- [35] The MathWorks, *MATLAB 7*, r2013b edition, 2013.
- [36] R. Minster, A. K. Saibaba and M. E. Kilmer, Randomized algorithms for low-rank tensor decompositions in the Tucker format, *SIAM J. Math. Data Sci.*, **2** (2020), 189–215.
- [37] J. Murray, *Mathematical biology II: spatial models and biomedical applications*, vol. 3, Springer-Verlag, 2001.
- [38] F. Negri, A. Manzoni and D. Amsallem, Efficient model reduction of parametrized systems by matrix discrete empirical interpolation, *J. Comput. Phys.*, **303** (2015), 431–454.
- [39] N.-C. Nguyen, A. T. Patera and J. Peraire, A ‘best points’ interpolation method for efficient approximation of parametrized functions, *Int J Numer Methods Eng*, **73** (2008), 521–543.
- [40] D. Palitta and V. Simoncini, Matrix-equation-based strategies for convection–diffusion equations, *BIT Numerical Mathematics*, **56** (2016), 751–776.
- [41] A. T. Patera and G. Rozza, *Reduced basis approximation and a posteriori error estimation for parametrized partial differential equations*, MIT Cambridge, MA, USA, 2007.

- [42] A. Quarteroni, *Numerical Models for Differential Problems*, vol. 8 of MS&A - Modeling, Simulation and Applications, Springer-Verlag, Milan, 2017.
- [43] S. J. Ruuth, Implicit-explicit methods for reaction-diffusion problems in pattern formation, *Journal of Mathematical Biology*, **34** (1995), 148–176.
- [44] S. Sahyoun and S. M. Djouadi, Nonlinear model reduction using space vectors clustering POD with application to the Burgers’ equation, in *2014 American Control Conference*, IEEE, 2014, 1661–1666.
- [45] J. A. Sherratt and M. A. Chaplain, A new mathematical model for avascular tumour growth, *J Math Biol*, **43** (2001), 291–312.
- [46] V. Simoncini, Numerical solution of a class of third order tensor linear equations, *BUMI*, **13** (2020), 429–439.
- [47] V. Simoncini, Computational methods for linear matrix equations, *SIAM Rev*, **58** (2016), 377–441.
- [48] R. Ștefănescu, A. Sandu and I. M. Navon, Comparison of POD reduced order strategies for the nonlinear 2D shallow water equations, *Int. J. Numer. Methods Fluids*, **76** (2014), 497–521.
- [49] J. C. Strikwerda, *Finite difference schemes and partial differential equations*, SIAM, 2004.
- [50] A. Tveito, H. P. Langtangen, B. F. Nielsen and X. Cai, *Elements of Scientific Computing*, Texts in Computational Science and Engineering, Springer-Verlag, Berlin, 2010.
- [51] V. K. Vanag, Waves and patterns in reaction–diffusion systems. Belousov–Zhabotinsky reaction in water-in-oil microemulsions, *Phys. Usp.*, **47** (2004), 923.
- [52] N. Vannieuwenhoven, R. Vandebril and K. Meerbergen, A new truncation strategy for the higher-order singular value decomposition, *SIAM J. Sci. Comput.*, **34** (2012), A1027–A1052.
- [53] Y. Wang, I. M. Navon, X. Wang and Y. Cheng, 2D Burgers equation with large Reynolds number using POD/DEIM and calibration, *Int. J. Numer. Methods Fluids*, **82** (2016), 909–931.

Received xxxx 20xx; revised xxxx 20xx.

E-mail address: gerhard.kirsten2@unibo.it